

A potential-flow BEM for large-displacement FSI

Citation for published version (APA):

Opstal, van, T. M., & Brummelen, van, E. H. (2012). *A potential-flow BEM for large-displacement FSI*. (CASA-report; Vol. 1203). Technische Universiteit Eindhoven.

Document status and date:

Published: 01/01/2012

Document Version:

Publisher's PDF, also known as Version of Record (includes final page, issue and volume numbers)

Please check the document version of this publication:

- A submitted manuscript is the version of the article upon submission and before peer-review. There can be important differences between the submitted version and the official published version of record. People interested in the research are advised to contact the author for the final version of the publication, or visit the DOI to the publisher's website.
- The final author version and the galley proof are versions of the publication after peer review.
- The final published version features the final layout of the paper including the volume, issue and page numbers.

[Link to publication](#)

General rights

Copyright and moral rights for the publications made accessible in the public portal are retained by the authors and/or other copyright owners and it is a condition of accessing publications that users recognise and abide by the legal requirements associated with these rights.

- Users may download and print one copy of any publication from the public portal for the purpose of private study or research.
- You may not further distribute the material or use it for any profit-making activity or commercial gain
- You may freely distribute the URL identifying the publication in the public portal.

If the publication is distributed under the terms of Article 25fa of the Dutch Copyright Act, indicated by the "Taverne" license above, please follow below link for the End User Agreement:

www.tue.nl/taverne

Take down policy

If you believe that this document breaches copyright please contact us at:

openaccess@tue.nl

providing details and we will investigate your claim.

A potential-flow BEM for large-displacement FSI

T.M. van Opstal and E.H. van Brummelen

Eindhoven University of Technology, Faculty of Mechanical Engineering, MEFD section

P.O. Box 513, 5600 MB Eindhoven, The Netherlands

March 2, 2012

ABSTRACT

This work concerns the interaction of light membrane structures enclosing incompressible fluids. Large displacements and collapsed boundaries (initially slender subdomains) are characteristic of this class of problems. A finite-element/boundary-element (FE/BE) coupled discretization is discussed in this work which addresses these challenges. Most common linear fluid models have a boundary-integral representation, restricting the problem to the boundary and making them amenable to a boundary element method (BEM) discretization. A marked advantage of this representation with respect to the conventional partial-differential-equation-based view of finite-element methods for fluids is the bypassing of volumetric meshing. The FE/BE approach is therefore an enabling method for fluid–structure interaction (FSI) problems involving membranes, and the present work serves as a proof of concept for this approach. Numerical experiments show the capabilities of the proposed scheme.

Keywords and Phrases: Fluid–structure interaction, inflatable structures, BEM, strong coupling

1. Introduction

Inflatable structures appear in a wide variety of engineering applications, e.g., evacuation slides in aircraft, air beams for temporary civil structures, stowable space structures, parachutes and air cushions. One of the most prominent examples of an inflatable structure is the airbag. Airbags form an indispensable component of passenger-safety systems in modern cars. Statistics of the US National Highway Traffic Safety Agency (NHTSA) corroborate that airbags yield a significant reduction in the fatality risk in frontal crashes, provided that the passenger is in position with respect to the airbag. On the other hand, NHTSA investigations have shown that airbags can form an important safety *risk* in out-of-position situations. Airbags deploy at more than 300 km/h with an impact force exceeding 5 kN and, hence, an airbag can severely injure or kill a passenger if impact occurs before full deployment. Incentivized by the danger of airbags in out-of-position situations, the NHTSA has issued new regulations that require car manufacturers to develop auxiliary restraint systems and new airbag systems to prevent such situations.

Numerical airbag-deployment simulations can provide valuable information in the assessment and control of out-of-position risks. Reliable numerical simulation of airbag-deployment dynamics is a complicated endeavor, however, on account of the inherent multiscale character of the inflation process. The initial stowed or folded configuration of the airbag forms a complex labyrinth of small folds with a characteristic length scale that is orders of magnitude smaller than that of the bulbous final configuration. On the macroscale associated with the final configuration, the flow of the inflator gas exhibits highly complex behavior, on account of its multi-component composition, high temperature gradients, and a wide spectrum of flow velocities, extending over subsonic, transonic and supersonic regimes. On the microscale pertaining to the small folds, compressibility effects are negligible and the flow exhibits relatively simple behavior. The complexity of the airbag-deployment process is further compounded by self-contact of the airbag fabric, which is particularly manifest in the initial stages of the deployment process. Hence, airbag-deployment processes constitute FSI problems with contact, in which the characteristic length scale of the geometry changes by many orders of magnitude, and

each of the length scales must be adequately resolved in the numerical method to arrive at a reliable prediction of the dynamical behavior.

Many related and challenging FSI computations have been performed with a wide array of methods, such as interface tracking [20, 30, 35] and interface capturing [6, 17, 25, 40] techniques. Intrinsically, these methods, being based on discretizations of the volume occupied by the fluid, are not employed in the analysis of realistic stowed configurations on account of the geometrical complexity of the domain as well as the very large displacements. For that reason, in industrial applications the load on the airbag fabric is determined by overly simplified fluid models, e.g., uniform-pressure models or empirical expressions. Such simplified models lack detailed information about the underlying physical processes, and generally cannot capture and predict the phenomena observed during experiments [24]. Recently, computational methods composed of particle-based approximation methods for the fluid, analogous to smoothed-particle hydrodynamics [27], have emerged [18]. The resolution provided by the moving particles in such approaches is uncontrollable, however, and on account of the large displacements that occur in airbag-deployment processes, the accuracy of particle-based methods is questionable.

The fundamental conundrum in airbag-deployment simulations, is that the scale disparity is so severe that the volumetric approximation methods that are suitable on the macroscale, cannot be employed on the microscale. The geometric complexity of the initial configuration precludes volumetric meshing with adequate resolution, even with adaptive interface-capturing or interface-tracking techniques [6, 17]. However, conversely, the flow model that underlies volumetric approximation methods, viz., the Euler or Navier-Stokes equations, appears unnecessarily sophisticated for the flow in the small-scale features of the airbag. It is anticipated that the flow in small-scale features can be represented by a simplified model, without essentially degrading the accuracy of the prediction of the dynamics of the airbag on the large scales. Airbag-deployment simulation therefore necessitates an adaptive multiscale approach of type-A [12] in which the flow in the small-scale features of the airbag is resolved by a different model than the flow in the large-scale features.

The boundary-integral equation can be conceived of as a microscale model for the fluid flow in small-scale features of airbags or, more generally, inflatable structures. In the present work, we consider a FSI model for inflatable structures based on a boundary-integral formulation of the fluid. We restrict our considerations to a 2D potential-flow model, but the investigation extends *mutatis mutandis* to for instance Stokes flow, which is treated in [28]. The connection to a macroscale model for the flow in the large-scale features and the corresponding model adaptivity will be treated in forthcoming work. The essential attribute of the boundary-integral formulation is that it provides an adequate model for the flow in the small-scale features of airbags, which does not require a volumetric mesh. In particular, the boundary-integral equation is set on the manifold of codimension one formed by the fluid-structure interface. The corresponding BEM is therefore invulnerable to the extreme deformations that occur in airbag-deployment processes. An additional advantage of the boundary-integral formulation in the context of FSI problems, is that it provides a very efficient model, as the domain of the flow model is restricted to the domain where the interaction with the structure actually occurs, viz., the fluid-structure interface.

The membrane in 2D is modeled as a linearly-elastic string [2, 39], regularized by a small flexural rigidity. The membrane equation is approximated by means of a standard finite-element discretization based on Hermite polynomials. Accordingly, the approximation of the aggregated FSI problem consists of an FE/BE coupled discretization. Contiguous use of FE/BE methods to exploit the advantages of both approaches, is an established practice; for a review see [33, 41]. Applications include blood flow [36], elasto-plasticity [13], crack propagation [29] and electromagnetics [34], amongst others. Coupled FE/BE approaches have also been applied to FSI problems in, e.g., [4, 5, 9, 11], but the application of FE/BE has so far been restricted to FSI problems with small deformations. The novelty of the present contribution lies in the exploitation of the boundary integral formulation in a new manner, viz., to enable very large deformations.

The remainder of this paper is organized as follows. Section 2 contains a statement of the considered fluid-membrane-interaction problem. Section 3 presents details of the discrete approximations and of

the iterative solution procedure for the aggregated FSI problem with contact. In section 4, we conduct numerical experiments to exemplify the properties of the BEM for fluid-membrane-interaction problems with large displacements. Finally, section 5 presents concluding remarks.

2. Problem statement

In this section, we present the mathematical formulation of the considered FSI problem with contact. Section 2.1 considers the boundary-integral formulation for the fluid subproblem, consisting of an irrotational, incompressible flow. Section 2.2 is concerned with the structure subproblem. The interface conditions which provide for the connection between the fluid and the structure are specified in section 2.3.

2.1 Boundary-integral formulation of the fluid subproblem

We consider a time-dependent open bounded domain $\Omega_t \subset \mathbb{R}^2$ with almost everywhere C^1 continuous boundary $\partial\Omega_t$. The boundary consists of the disjoint union of the time-dependent wet boundary Γ_t and the fixed inflow boundary Γ_{in} . We assume that the initial configuration of the boundary is specified by means of an arc-length parametrization conforming to:

$$\Gamma_0 = \{\mathbf{x} \in \mathbb{R}^2 : \mathbf{x} = \boldsymbol{\chi}_0(s), s \in (0, L)\}, \quad \Gamma_{\text{in}} = \{\mathbf{x} \in \mathbb{R}^2 : \mathbf{x} = \boldsymbol{\chi}_0(s), s \in (L, \Lambda)\}, \quad (2.1)$$

and $|\partial_s \boldsymbol{\chi}_0(s)| = 1$. Denoting by $\mathbf{z} := \mathbf{z}_t(\cdot) := [\mathbf{z}(t)](\cdot) := \mathbf{z}(t, \cdot)$ the position of the material point on the boundary with initial position $\boldsymbol{\chi}_0(\cdot)$, the boundary at time t is parametrized with respect to the arc length of the initial configuration according to $\partial\Omega_t = \{\mathbf{x} \in \mathbb{R}^2 : \mathbf{x} = \mathbf{z}_t(s), s \in (0, \Lambda)\}$; see figure 1 for an illustration. Because the inflow boundary is fixed, it holds that $\mathbf{z}_t(s) = \boldsymbol{\chi}_0(s)$ for $s \in (L, \Lambda)$.

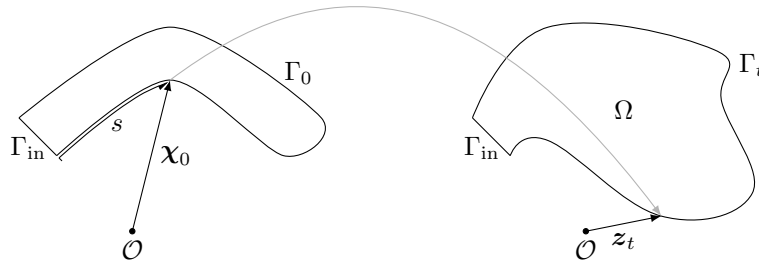


Figure 1: Schematized problem geometry.

The fluid subproblem consists of the irrotational flow of an incompressible fluid on the time-dependent domain Ω_t . Accordingly, there exists a harmonic potential $\phi : \Omega_t \rightarrow \mathbb{R}$ such that the fluid velocity \mathbf{v} coincides with $\nabla\phi$. The wetted boundary Γ_t corresponds to a material boundary of the fluid domain, which implies that the normal velocity of the fluid coincides with the velocity of the boundary in its normal direction. Moreover, on the inflow boundary Γ_{in} , we have a prescribed normal velocity. The boundary conditions for the fluid translate into Neumann-type conditions for the potential. The fluid is therefore described by the Laplace–Neumann problem:

$$-\Delta\phi = 0 \quad \text{in } \Omega_t, \quad (2.2a)$$

$$\partial_{\mathbf{n}}\phi = h \quad \text{on } \partial\Omega_t, \quad (2.2b)$$

where Δ denotes the Laplace operator and $h : \partial\Omega_t \rightarrow \mathbb{R}$ represents time-dependent exogenous data. To connect the fluid to the structure in the aggregated FSI problem, we shall be exclusively interested in the trace of ϕ on $\partial\Omega_t$. It is to be noted that (2.2) complies with a Fredholm alternative: existence of a solution to (2.2) is contingent on the condition that $\oint h = 0$, and the solution is unique only up to a constant; see also section 2.4.

Given the structure of (2.2) and our restricted interest in the trace of ϕ , we can cast the Laplace–Neumann problem into a boundary-integral formulation. Various formulations of this type exist, viz., the direct formulation, and single-layer and double-layer formulations; see for instance [8]. To facilitate the connection with the membrane in the aggregated FSI problem, the following direct formulation is most suitable:

$$a\phi + K\phi = Vh \quad \text{on } \partial\Omega_t, \quad (2.3)$$

where $a(\mathbf{x})$ is the interior angle between the left and right one-sided limits of the tangent vector at \mathbf{x} divided by 2π . In particular, $a = 1/2$ on smooth parts of the boundary. The operators $K(\cdot)$ and $V(\cdot)$, generally referred to as the *single-layer potential* and the *double-layer potential*, respectively, correspond to (traces of) convolutions with singular kernels:

$$(Vh)(\mathbf{x}) := \oint_{\partial\Omega_t} G(\mathbf{x}, \mathbf{y}) h(\mathbf{y}) d\sigma_t(\mathbf{y}), \quad (2.4a)$$

$$(K\phi)(\mathbf{x}) := \oint_{\partial\Omega_t} \partial_{\mathbf{n}} G(\mathbf{x}, \mathbf{y}) \phi(\mathbf{y}) d\sigma_t(\mathbf{y}), \quad (2.4b)$$

where G denotes the Green’s function for the negative Laplace operator in \mathbb{R}^2 ,

$$G(\mathbf{x}, \mathbf{y}) := -(2\pi)^{-1} \log |\mathbf{x} - \mathbf{y}|, \quad (2.5)$$

and $d\sigma_t$ denotes the measure carried by the boundary $\partial\Omega_t$. Moreover, $\partial_{\mathbf{n}} G(\mathbf{x}, \mathbf{y})$ stands for the conormal derivative of the Green’s function with respect to its second argument:

$$\partial_{\mathbf{n}} G(\mathbf{x}, \mathbf{y}) := (2\pi)^{-1} |\mathbf{x} - \mathbf{y}|^{-2} (\mathbf{x} - \mathbf{y}) \cdot \mathbf{n}(\mathbf{y}). \quad (2.6)$$

The double-layer potential is to be understood in the *Cauchy-principal-value* sense; see, e.g., [19, 26, 31]. A derivation of the above boundary-integral form of (2.2) can be found in, for instance, Refs. [22, 38].

To enable a more precise interpretation of (2.3), we denote by $H^1(\Omega_t)$ the Sobolev space of square-integrable functions with square-integrable distributional derivatives, by $H^{1/2}(\partial\Omega_t)$ the image of the trace operator on $H^1(\Omega_t)$, and by $H^{-1/2}(\partial\Omega_t)$ the dual space of $H^{1/2}(\partial\Omega_t)$. Let us note that the space $H^1(\Omega_t)$, and its trace and the dual thereof, are well defined whenever Ω_t corresponds to a Lipschitz transformation of a fixed Lipschitz domain, because H^1 is invariant with respect to such transformations. The data h in (2.2) corresponds to an element of $H^{-1/2}(\partial\Omega_t)$. The function ϕ in the left member of (2.3) is the trace of a function in $H^1(\Omega_t)$ and, accordingly, it resides in $H^{1/2}(\partial\Omega_t)$. An important result due to Costabel [7, Thm. 1] is that the single-layer potential $V : H^{-1/2}(\partial\Omega_t) \rightarrow H^{1/2}(\partial\Omega_t)$ and the double-layer potential $K : H^{1/2}(\partial\Omega_t) \rightarrow H^{1/2}(\partial\Omega_t)$ are continuous. Hence, equation (2.3) can be conceived of as an identity of elements in $H^{1/2}(\partial\Omega_t)$.

The Fredholm alternative that holds for the Laplace–Neumann problem (2.2) also applies to the boundary-integral formulation (2.3), as $a + K$ has a nontrivial kernel consisting of constant functions and the image of $a + K$ does not contain constant functions other than 0; cf. also Appendix B. We consider a weak formulation of (2.3), in which the constant functions are removed from the test and trial spaces. Let $L^2(\partial\Omega_t)$ denote the Hilbert space of real-valued square-integrable functions on $\partial\Omega_t$, equipped with the inner product $(\phi, \psi)_{L^2(\partial\Omega_t)} = \int_{\partial\Omega_t} \phi \psi$. The inner product $(\cdot, \cdot)_{L^2(\partial\Omega_t)}$ extends by continuity to a duality pairing on $H^{1/2}(\partial\Omega_t) \times H^{-1/2}(\partial\Omega_t)$ or $H^{-1/2}(\partial\Omega_t) \times H^{1/2}(\partial\Omega_t)$. Denoting by $H_{\oint=0}^{\pm 1/2}(\partial\Omega_t) := \{\psi \in H^{\pm 1/2}(\partial\Omega_t) : (\psi, 1)_{L^2(\partial\Omega_t)} = 0\}$ the class of distributions in $H^{\pm 1/2}(\partial\Omega_t)$ orthogonal to constants, the boundary-integral formulation (2.3) can be cast into the weak form:

$$\text{find } \phi \in H_{\oint=0}^{1/2}(\partial\Omega_t) : \quad a_{\text{f}}(\phi, \psi) = b_{\text{f}}(\psi) \quad \forall \psi \in H_{\oint=0}^{-1/2}(\partial\Omega_t), \quad (2.7)$$

where the bilinear form $a_{\text{f}} : H^{1/2}(\partial\Omega_t) \times H^{-1/2}(\partial\Omega_t) \rightarrow \mathbb{R}$ and the linear form $b_{\text{f}} : H^{-1/2}(\partial\Omega_t) \rightarrow \mathbb{R}$ are defined by:

$$a_{\text{f}}(\phi, \psi) = \left(\frac{1}{2}\phi + K\phi, \psi\right)_{L^2(\partial\Omega_t)}, \quad b_{\text{f}}(\psi) = (Vh, \psi)_{L^2(\partial\Omega_t)}. \quad (2.8)$$

The bilinear form $a_f(\cdot, \cdot)$ and linear form $b_f(\cdot)$ according to (2.8) are continuous. From [31, Thms. 3.8.7 and 3.8.9] it moreover follows that:

$$C_K \|\phi\|_{H^{1/2}(\partial\Omega_t)} \leq \|\frac{1}{2}\phi + K\phi\|_{H^{1/2}(\partial\Omega_t)} \quad \forall \phi \in H_{\mathcal{f}=0}^{1/2}(\partial\Omega_t), \quad (2.9a)$$

$$C_K \|\psi\|_{H^{-1/2}(\partial\Omega_t)} \leq \|\frac{1}{2}\psi + K'\psi\|_{H^{-1/2}(\partial\Omega_t)} \quad \forall \psi \in H_{\mathcal{f}=0}^{-1/2}(\partial\Omega_t), \quad (2.9b)$$

with $K' : H^{-1/2}(\partial\Omega_t) \rightarrow H^{-1/2}(\partial\Omega_t)$ the dual operator corresponding to K , and C_K a positive constant. These lower bounds on the norms of $\frac{1}{2}I + K$ and $\frac{1}{2}I + K'$ imply that the bilinear form $a_f(\cdot, \cdot)$ satisfies:

$$\inf_{\phi \in H_{\mathcal{f}=0}^{1/2}(\partial\Omega_t) \setminus \{0\}} \sup_{\psi \in H_{\mathcal{f}=0}^{-1/2}(\partial\Omega_t) \setminus \{0\}} \frac{|a_f(\phi, \psi)|}{\|\phi\|_{H^{1/2}(\partial\Omega_t)} \|\psi\|_{H^{-1/2}(\partial\Omega_t)}} \geq C_f > 0, \quad (2.10a)$$

$$\forall \psi \in H_{\mathcal{f}=0}^{-1/2}(\partial\Omega_t) \setminus \{0\} : \sup_{\phi \in H_{\mathcal{f}=0}^{1/2}(\partial\Omega_t) \setminus \{0\}} |a_f(\phi, \psi)| > 0, \quad (2.10b)$$

for some constant C_f . The bilinear form and the linear form therefore comply with the conditions of the Banach-Nečas-Babuška (BNB) theorem [14, Thm. 2.6], which implies that there exists a unique and stable solution to (2.7).

Although $H_{\mathcal{f}=0}^{1/2}(\partial\Omega_t) \times H_{\mathcal{f}=0}^{-1/2}(\partial\Omega_t)$ is the natural setting of the weak formulation of the boundary-integral formulation, in view of the connection to the underlying Laplace-Neumann problem, an alternative weak formulation in $L_{\mathcal{f}=0}^2(\partial\Omega_t) = \{\phi \in L^2(\partial\Omega_t) : (\phi, 1)_{L^2(\partial\Omega_t)} = 0\}$ can be established. Theorem 1 in [7] (see also [31, §3.1.2]) asserts, more precisely, that $K : H^{1/2+\varsigma}(\partial\Omega_t) \rightarrow H^{1/2+\varsigma}(\partial\Omega_t)$ is a continuous linear operator for any $\varsigma \in [-1/2, 1/2]$. Therefore, we can conceive of (2.7) as a weak formulation on $L_{\mathcal{f}=0}^2(\partial\Omega_t) \times L_{\mathcal{f}=0}^2(\partial\Omega_t)$,

$$\text{find } \phi \in L_{\mathcal{f}=0}^2(\partial\Omega_t) : \quad a_f(\phi, \psi) = b_f(\psi) \quad \forall \psi \in L_{\mathcal{f}=0}^2(\partial\Omega_t), \quad (2.11)$$

if, accordingly, the bilinear form $(\cdot, \cdot)_{L^2(\partial\Omega_t)}$ in the definition of a_f and b_f in (2.8) is interpreted as a standard L^2 inner product, and not the extension to a duality pairing; see also [31, §3.8]. The BNB conditions (2.10) must then also be assessed with respect to $L_{\mathcal{f}=0}^2(\partial\Omega_t)$.

Regarding Galerkin finite-element discretizations of (2.7) or (2.11), it is to be noted that standard conforming discretizations of the two formulations can be distinct, as discretizations of (2.7) have to be $H^{1/2}(\partial\Omega_t)$ conforming, while discretizations of (2.11) only have to be $L^2(\partial\Omega_t)$ conforming. For instance, a conforming approximation to (2.7) would have to be continuous, while a conforming approximation to (2.11) does not. Approximations of (2.7) and (2.11) based on $H^{1/2}(\partial\Omega_t)$ -conforming finite-element spaces are evidently identical. Furthermore, various Galerkin approximations can be derived from (2.7), based on reformulations which are equivalent in the continuous case. For instance, by virtue of Riesz representation theorem (e.g. [31, Thm. 2.1.17]) and the fact that $\frac{1}{2}I + K : H_{\mathcal{f}=0}^{1/2}(\partial\Omega_t) \rightarrow H_{\mathcal{f}=0}^{1/2}(\partial\Omega_t)$ constitutes an isomorphism, (2.7) is equivalent to:

$$\begin{aligned} \text{find } \phi \in H_{\mathcal{f}=0}^{1/2}(\partial\Omega_t) : \quad & (\frac{1}{2}\phi + K\phi, \frac{1}{2}\psi + K\psi)_{H^{1/2}(\partial\Omega_t)} \\ & = (Vh, \frac{1}{2}\psi + K\psi)_{H^{1/2}(\partial\Omega_t)} \quad \forall \psi \in H_{\mathcal{f}=0}^{1/2}(\partial\Omega_t). \end{aligned} \quad (2.12)$$

The advantage of the formulation (2.12) is that the bilinear form in this formulation is (strongly) coercive; see (2.9a). Because coercivity transfers to subspaces, any conforming discretization of (2.12) satisfies the conditions of the Lax–Milgram lemma and is hence stable. Conversely, the BNB conditions (2.10) do not generally transfer to subspaces, and these conditions have to be reassessed for the finite-element approximation spaces. The computation of the $H^{1/2}$ -inner products in (2.12) is intricate, however, which limits the practical use of this formulation in finite-element approximations.

For this reason, below we consider $H^{1/2}(\partial\Omega_t)$ -conforming finite-element approximations of (2.7) or, equivalently, (2.11). Moreover, to further facilitate the implementation, we remove the orthogonality condition $(\cdot, 1)_{L^2(\partial\Omega_t)} = 0$ from the test- and trial-spaces and instead impose it by means of Lagrange multipliers.

2.2 Structure subproblem

The wet boundary of the fluid is composed of a membrane corresponding to a regularized linearly-elastic string:

$$\mathbf{z}'' - D(D\mathbf{z}(1 - |D\mathbf{z}|^{-1})) + \epsilon D^4 \mathbf{z} = \mathbf{f} \quad \text{on } (0, L), \quad (2.13)$$

where $\mathbf{z} : (0, L) \rightarrow \mathbb{R}^2$ denotes the position of the membrane parametrized with respect to the arc-length coordinate of the initial configuration, and D denotes the (distributional) derivative, $[D\mathbf{z}(t)](s) = \partial\mathbf{z}(t, s)/\partial s$. The load \mathbf{f} depends implicitly on \mathbf{z} due to contact forces and fluid loads; see equation (2.16) below. The first two terms in the left member of (2.13) correspond to a linearly-elastic string. The final term yields a regularization, which is required to avoid instability in compression, i.e., when $|D\mathbf{z}| \leq 1$. The string equation in (2.13) can be derived from the general equations of motion of an elastic solid under the assumptions of line-stress and linear elasticity and, in particular, the strain term corresponds to a strain energy $\Psi = E + 1 - \sqrt{2E + 1}$ with $E = (|D\mathbf{z}|^2 - 1)/2$ the Green-Lagrange strain tensor. Equation (2.13) is in fact in nondimensional form. The nondimensionalization is elaborated in appendix A.

Equation (2.13) must be complemented with suitable initial and boundary conditions. The membrane is attached to hinged supports, which fix the position of the membrane without inducing moments:

$$\mathbf{z}(s) = \boldsymbol{\chi}_0(s), \quad D^2 \mathbf{z}(s) = 0 \quad \text{for } s \in \{0, L\}. \quad (2.14)$$

The initial conditions on the position of the membrane are provided by

$$\mathbf{z}|_{t=0} = \boldsymbol{\chi}_0, \quad \mathbf{z}'|_{t=0} = \boldsymbol{\chi}_1, \quad (2.15)$$

where $\boldsymbol{\chi}_0$ refers to the initial configuration and $\boldsymbol{\chi}_1$ represents a prescribed initial velocity.

The load on the membrane consists of the fluid traction, proportional to pressure p , and the contact force. The fluid traction induces a load in the normal direction of the membrane. The contact force is represented by a nonlinear operator, F , which associates to any configuration a load on that configuration; see section 2.5. The load \mathbf{f} can be separated into

$$\mathbf{f} := |D\mathbf{z}|(p \circ \mathbf{z} \mathbf{n}_z \circ \mathbf{z} + \boldsymbol{\varphi}_z \circ \mathbf{z}) = p \circ \mathbf{z} \operatorname{rot} D\mathbf{z} + |D\mathbf{z}| \boldsymbol{\varphi}_z \circ \mathbf{z}, \quad (2.16)$$

with $\operatorname{rot} : \mathbb{R}^2 \rightarrow \mathbb{R}^2$ the rotation operator, $\operatorname{rot}(a_1, a_2) = (a_2, -a_1)$. It is to be noted that the normal vector depends explicitly on the configuration. The composition of p , \mathbf{n}_z and $\boldsymbol{\varphi}_z$ with \mathbf{z} serves to transport the pressure, the normal vector and the contact load to the parameterized interval $(0, L)$. The multiplication by $|D\mathbf{z}|$ accounts for the ratio of the surface measures in the initial and the actual configuration.

We proceed with a more precise specification of (2.13)–(2.16). To this end, we require some elementary notational conventions. We denote by $\mathbf{L}^p(0, L)$ ($1 \leq p < \infty$) the Lebesgue space of functions from $(0, L)$ into \mathbb{R}^2 with p -integrable Euclidean norm, equipped with the norm $\|\cdot\|_{\mathbf{L}^p(0, L)} = (\int_0^L |\cdot|^p)^{1/p}$. For $p = \infty$, the above definition is extended by setting $\|\mathbf{z}\|_{\mathbf{L}^\infty(0, L)} = \operatorname{ess\,sup}\{|\mathbf{z}(s)| : s \in (0, L)\}$. Furthermore, we denote by $\mathbf{W}^{m, p}(0, L)$ the Sobolev space of functions $\mathbf{z} \in \mathbf{L}^p(0, L)$ with distributional derivatives $D^k \mathbf{z} \in \mathbf{L}^p(0, L)$ for all $k \leq m$. The spaces $\mathbf{L}^2(0, L)$ and $\mathbf{H}^m(0, L) := \mathbf{W}^{m, 2}(0, L)$ ($m \in \mathbb{Z}_+$) are Hilbert spaces when provided with the inner products

$$(\mathbf{w}, \mathbf{z})_{\mathbf{L}^2(0, L)} = \int_0^L \mathbf{w}(s) \cdot \mathbf{z}(s) ds, \quad (\mathbf{w}, \mathbf{z})_{\mathbf{H}^2(0, L)} = (\mathbf{w}, \mathbf{z})_{\mathbf{L}^2(0, L)} + \sum_{k=1}^2 (D^k \mathbf{w}, D^k \mathbf{z})_{\mathbf{L}^2(0, L)}.$$

The subspace of $\mathbf{H}^m(0, L)$ ($m \in \mathbb{N}$) of functions that vanish on the boundary $\{0, L\}$ is represented by $\mathbf{H}_0^m(0, L)$. For notational convenience we deviate from the standard notation $\mathbf{H}^m(0, L) \cap \mathbf{H}_0^1(0, L)$. Considering a time interval $(0, T)$ and a normed space $(\mathbf{B}, \|\cdot\|_{\mathbf{B}})$, we denote by $L^q(0, T; \mathbf{B})$ ($1 \leq q < \infty$) the Bochner space of functions $\mathbf{z} : (0, T) \rightarrow \mathbf{B}$ such that the function $t \mapsto \|\mathbf{z}(t)\|_{\mathbf{H}}$ is q -integrable, equipped with the norm $\|\mathbf{z}\|_{L^q(0, T; \mathbf{B})} = (\int_0^T \|\mathbf{z}(t)\|_{\mathbf{B}}^q dt)^{1/q}$. These definitions are extended to $q = \infty$ by setting $\|\mathbf{z}\|_{L^\infty(0, T; \mathbf{B})} = \text{ess sup}\{\|\mathbf{z}(t)\|_{\mathbf{B}} : t \in (0, T)\}$.

On account of the nonlinear dependence of the stress $(1 - |D\mathbf{z}|^{-1})$ and of the load vector \mathbf{f} in (2.16) on \mathbf{z} , a precise specification of the domain of the structure operator is nontrivial. The principal part of the operator, corresponding to the regularizing term $\epsilon D^4(\cdot)$, is however linear and elliptic. We shall assume that the character of the principal part extends to the nonlinear structure operator. Restricting our consideration to the principal part of the structure operator, equation (2.13) corresponds to an evolution equation of the second order (in t) with an elliptic operator ϵD^4 from $\mathbf{H}_0^2(0, L)$ into its dual space $\mathbf{H}^{-2}(0, L)$. A comprehensive general theory is available for evolution equations of this type; see, for instance, [10, 15, 23]. We defer the result $\mathbf{f} \in L^2(0, T; \mathbf{H}^{-2}(0, L))$ to section 2.5, where the contact force is treated. Ignoring the nonlinear term in (2.13), and insisting that $\boldsymbol{\chi}_0 \in \mathbf{H}_0^2(0, L)$ and $\boldsymbol{\chi}_1 \in \mathbf{L}^2(0, L)$, equation (2.13) subject to (2.14) and (2.15) defines a unique solution in $\boldsymbol{\chi}_0 + W(0, T)$, with $W(0, T)$ the collection of admissible structure displacements:

$$W(0, T) = \{\mathbf{w} \in L^2(0, T; \mathbf{H}_0^2(0, L)) : \mathbf{w}' \in L^2(0, T; \mathbf{L}^2(0, L))\}. \quad (2.17)$$

Moreover, it holds that $\mathbf{z}'' \in L^2(0, T; \mathbf{H}^{-2}(0, L))$. The left and right members of (2.13) therefore admit an unambiguous interpretation as elements of $L^2(0, T; \mathbf{H}^{-2}(0, L))$.

We assume that the setting of the structural position in (2.17) can be retained for the nonlinear operator. However, in addition, we assume that $|D\mathbf{z}|$ is almost everywhere bounded from below, i.e., $|D\mathbf{z}| \geq \alpha > 0$, and that $\mathbf{z}(t) : (0, L) \rightarrow \Gamma_t$ is bijective for all $t \in (0, T)$. The first assumption reflects that parts of the membrane that initially have finite extent do not vanish during the motion. The second assumption prohibits self-intersection of the membrane.

The general theory for evolution equations of the second order in [23, §3.8.4] provides a refined regularity result for the solution to (2.13)–(2.15). Under the above conditions on the data, the displacement and the velocity can be conceived of as continuous-in-time functions, taking values in $\mathbf{H}_0^2(0, L)$ and $\mathbf{L}^2(0, L)$, respectively, and the solution to (2.13)–(2.15) in fact satisfies

$$\mathbf{z} \in \boldsymbol{\chi}_0 + \{\mathbf{w} \in L^\infty(0, T; \mathbf{H}_0^2(0, L)) : \mathbf{w}' \in L^\infty([0, T]; \mathbf{L}^2(0, L))\}. \quad (2.18)$$

This refined regularity result is important to assign significance to the transmission conditions in the aggregated FSI problem; see section 2.3.

It is to be remarked that the above elementary model for a membrane is in fact surprisingly difficult to analyze. Refs. [2, 39] derive the model (without regularization) without regard for the complications related to compression. Results on existence and uniqueness appear to be nonexistent; see also [1].

2.3 Transmission conditions

The fluid and the structure interact at their mutual interface via so-called transmission conditions. These transmission conditions can be separated into a dynamic condition, which specifies continuity of tractions, and a kinematic condition, which expresses continuity of motion. The kinematic condition imposes that on the wetted boundary Γ_t , the normal velocity of the fluid coincides with the normal velocity of the membrane. Indicating the normal velocity on the inflow boundary Γ_{in} by q , the kinematic condition translates into the following specification of the Neumann data h in (2.2):

$$h = \begin{cases} \mathbf{n}_{\mathbf{z}} \cdot (\mathbf{z}' \circ \mathbf{z}^{-1}) & \text{at } \Gamma_t, \\ q & \text{at } \Gamma_{\text{in}}. \end{cases} \quad (2.19)$$

The composition of \mathbf{z}' with \mathbf{z}^{-1} serves to transport \mathbf{z}' to Γ_t .

The dynamic condition imposes continuity of tractions at the fluid-structure interface. The pressure can be extracted from Bernoulli's principle. Restricting our consideration to quasi-static flows, which allows us to suppress the time-dependence of the potential in Bernoulli's relation, it follows that the pressure p in the structure load according to (2.16) is related to the flow potential by:

$$p := p(\phi) = p_0 - \frac{1}{2}\vartheta|\nabla\phi|^2 = p_0 - \frac{1}{2}\vartheta(\mathbf{z}' \cdot (|D\mathbf{z}|^{-1}\text{rot } D\mathbf{z}))^2 \circ \mathbf{z}^{-1} + \frac{1}{2}\vartheta|\nabla_{\Gamma}\phi|^2, \quad (2.20)$$

with ϑ the fluid-structure mass ratio and ∇_{Γ} the so-called *tangential gradient* (or Γ -*gradient*), formally, $\nabla_{\Gamma}\phi = \nabla\phi - \mathbf{n}\partial_{\mathbf{n}}\phi$. Moreover, p_0 represents a (possibly time-dependent) pressure level; cf. section 2.4. The final identity in (2.20) follows from a decomposition of the gradient into its normal and tangential components, in combination with (2.19).

To establish the suitability of the Neumann data in accordance with the kinematic condition, we will show that the data on the wet boundary resides in $L^{\infty}(0, T; L^2(\Gamma_t))$ and, a fortiori, that it defines a functional in $L^{\infty}(0, T; H^{-1/2}(\partial\Omega_t))$. By transporting the integral on Γ_t to the parameter interval $(0, L)$ and, subsequently, applying Hölder's inequality, we obtain:

$$\begin{aligned} \|h\|_{L^{\infty}(0, T; L^2(\Gamma_t))} &= \left\| \left(\int_{\Gamma_t} (\mathbf{n}_{\mathbf{z}} \cdot (\mathbf{z}' \circ \mathbf{z}^{-1}))^2 d\sigma_t \right)^{1/2} \right\|_{L^{\infty}(0, T)} \\ &\leq \left\| \left(\int_0^L |\mathbf{n}_{\mathbf{z}} \circ \mathbf{z}|^2 |\mathbf{z}'(\cdot, s)|^2 |D\mathbf{z}(\cdot, s)| ds \right)^{1/2} \right\|_{L^{\infty}(0, T)} \\ &\leq \|\mathbf{z}'\|_{L^{\infty}(0, T; L^2(0, L))} \|D\mathbf{z}\|_{L^{\infty}(0, T; L^{\infty}(0, L))}^{1/2}. \end{aligned} \quad (2.21)$$

In the final inequality we have taken into account that $|D\mathbf{z}|^{-1}|\text{rot } D\mathbf{z}| \leq 1$ almost everywhere. Sobolev's inequality (cf. for instance [, Thm. 1.4.6]) implies that the embedding $\mathbf{H}^1(0, L) \hookrightarrow \mathbf{L}^{\infty}(0, L)$ is continuous. The refined regularity result (2.18) then leads to the conclusion that, indeed, $\|h\|_{L^{\infty}(0, T; L^2(\Gamma_t))}$ is bounded.

To confirm that the dynamic condition is meaningful, we must show that the map

$$\mathbf{w} \mapsto \int_0^T \int_0^L \mathbf{w}(t, s) \cdot (p \circ \mathbf{z}(t, s) \text{rot } D\mathbf{z}(t, s)) ds dt, \quad (2.22)$$

with p according to Bernoulli's relation (2.20), corresponds to a continuous linear functional on $L^2(0, T; \mathbf{H}_0^2(0, L))$; cf. (2.16). Without loss of generality, we set $\vartheta = 1$. Anticipating that the pressure level p_0 resides in $L^2(0, T)$ (see section 2.4), we apply Hölder's theorem to bound the term corresponding to p_0 according to:

$$\left| \int_0^T \int_0^L p_0(t) \mathbf{w}(t, s) \cdot \text{rot } D\mathbf{z}(t, s) ds dt \right| \leq \|p_0\|_{L^2(0, T)} \|\mathbf{w}\|_{L^2(0, T; L^2(0, L))} \|D\mathbf{z}\|_{L^{\infty}(0, T; L^2(0, T))}.$$

By virtue of the refined regularity result (2.18), the p_0 -term is therefore indeed continuous. Moreover, by Hölder's inequality, the term corresponding to $(\partial_{\mathbf{n}}\phi)^2$ in (2.20) is bounded according to

$$\begin{aligned} \left| \int_0^T \int_0^L \mathbf{w}(t, s) \cdot \text{rot } D\mathbf{z}(t, s) (\mathbf{z}'(t, s) \cdot (\mathbf{n}_{\mathbf{z}} \circ \mathbf{z}))^2 ds dt \right| \\ \leq \|\mathbf{w}\|_{L^2(0, T; L^{\infty}(0, L))} \|D\mathbf{z}\|_{L^{\infty}(0, T; L^{\infty}(0, L))} \|\mathbf{z}'\|_{L^{\infty}(0, T; L^2(0, L))}^2, \end{aligned}$$

where we have again taken account of the fact that that $|D\mathbf{z}|^{-1}|\text{rot } D\mathbf{z}| \leq 1$ almost everywhere. The refined regularity result (2.18) and the continuity of the embedding of $\mathbf{H}^m(0, L) \hookrightarrow \mathbf{L}^{\infty}(0, L)$ ($m \in \mathbb{N}$)

then conveys that the term related to $(\partial_{\mathbf{n}}\phi)^2$ is indeed bounded. Hence, it remains to bound the term originating from the surface gradient in Bernoulli's relation. Hölder's inequality yields:

$$\left| \int_0^T \int_0^L \mathbf{w}(s) \cdot \operatorname{rot} D\mathbf{z}(s) (\nabla_{\Gamma}\phi)^2 \circ \mathbf{z}(s) ds dt \right| \leq \|\mathbf{w}\|_{L^2(0,T;L^\infty(0,L))} \|D\mathbf{z}\|_{L^\infty(0,T;L^\infty(0,L))} \|\nabla_{\Gamma}\phi \circ \mathbf{z}\|_{L^2(0,T;L^2(0,L))}^2.$$

Boundedness of the first two factors in the right member again follows from the refined regularity result and the aforementioned embedding relations, and it is now left to show that $\nabla_{\Gamma}\phi \circ \mathbf{z} \in L^2(0,T;L^2(0,L))$ or, in view of the fact that \mathbf{z} is essentially continuous, $\nabla_{\Gamma}\phi \in L^2(0,T;L^2(\Gamma_t))$. It is to be noted that such a result is cogent but non-standard, both in the context of the Neumann problem (2.2) and of the boundary-integral formulation (2.3). For the Neumann problem, we have the general result that for $h \in H^{-1/2}(\partial\Omega)$, it holds that $\phi \in H^1(\Omega)$ and $\nabla_{\Gamma}\phi \in H^{-1/2}(\partial\Omega)$; see, for instance, the review of trace operators in [32]. On domains with suitably smooth boundaries it furthermore holds that if the Neumann data has higher regularity, viz., $h \in H^{m+\frac{1}{2}}(\partial\Omega)$ ($m \in \mathbb{Z}_+$), then $\phi \in H^{m+2}(\Omega)$ and, accordingly, $\nabla_{\Gamma}\phi \in H^{m+\frac{1}{2}}(\partial\Omega)$; see [14, Thm. 3.10]. If we insist that the inflow data $q \in L^2(\Gamma_{\text{in}})$, then the Neumann data h resides in $L^2(\partial\Omega)$, and we require an intermediate result. Such a result is non-standard, however. The standard result for the boundary-integral formulation in [7] asserts that $\phi \in H^{1/2}(\partial\Omega)$ whenever $h \in H^{-1/2}(\partial\Omega)$, analogous to the general result for the Neumann problem; see also section 2.1. It is to be noted, however, that in [7] it is conjectured that higher-regularity results hold under auxiliary smoothness conditions on the domain. In appendix B, we establish that in the 1-dimensional setting under consideration, such a higher-regularity result indeed holds, under auxiliary assumptions on the domain.

2.4 Compatibility condition

The selection of the pressure level p_0 is not obvious. The pressure level is in fact related to an auxiliary coupling condition between the fluid and the structure, in addition to the aforementioned kinematic and dynamic interface conditions, which originates from the incompressibility of the fluid. The incompressibility of the fluid engenders a Fredholm alternative for the Laplace–Neumann problem (2.2). By the divergence theorem, we have the identities:

$$\int_{\Omega_t} \Delta\phi = \oint_{\partial\Omega_t} \partial_{\mathbf{n}}\phi = \oint_{\partial\Omega_t} h = 0. \quad (2.23)$$

Hence, the Laplace–Neumann problem admits a solution if and only if the data h complies with the compatibility condition $\oint h = 0$. Moreover, $\ker(\Delta, \partial_{\mathbf{n}}) = \operatorname{span}\{1\}$ and, hence, the solution to (2.2) is unique only up to an additive constant. On account of (2.19), the compatibility condition in (2.23) translates into a compatibility condition on the structure displacement. Such an auxiliary coupling between the fluid and the structure is typical for FSI problems with enclosed incompressible fluids; see also [21].

Denoting by $Q(\mathbf{z})$ the volume contained within a certain structure configuration \mathbf{z} and by $c(t)$ the content of the fluid domain,

$$c(t) = Q(\boldsymbol{\chi}_0) + \int_0^t \int_{\Gamma_{\text{in}}} q, \quad (2.24)$$

the structure displacement must comply with $Q(\mathbf{z}(t)) = c(t)$. We shall impose this compatibility condition in the weak formulation of (2.13)–(2.15) by means of a Lagrange multiplier. Moreover, to elucidate the relation between the pressure level, p_0 , and the compatibility condition, we separate \mathbf{f} in (2.13) in accordance with (2.16) and, subsequently, replace p in accordance with (2.20). We denote by

$$W_0(0, T) = \{\mathbf{z} \in W(0, T); \mathbf{z}|_{t=0} = 0\}, \quad (2.25a)$$

$$W_T(0, T) = \{\mathbf{z} \in W(0, T); \mathbf{z}|_{t=T} = 0\}, \quad (2.25b)$$

the admissible structure-displacement fields with vanishing initial and terminal traces, respectively. Let us remark that the trace of \mathbf{z} at $t = 0$ in (2.25a) is well defined in $\mathbf{L}^2(0, L)$; see, for instance, [14, 15, 23]. The structure-displacement problem, including the volume constraint, can then be condensed into the weak formulation: *find* $\mathbf{z} \in \boldsymbol{\chi}_0 + W_0(0, T)$, $\lambda \in L^2(0, T)$ *such that* $\forall \mathbf{w} \in W_T(0, T)$, $\mu \in L^2(0, T)$:

$$\begin{aligned} & - \int_0^T (\mathbf{z}'(t), \mathbf{w}'(t))_{\mathbf{L}^2(0,L)} dt + (\mathbf{z}'(T), \mathbf{w}(T))_{\mathbf{L}^2(0,L)} + \int_0^T a_s(\mathbf{z}(t); \mathbf{w}(t)) dt \\ & - \int_0^T p_0(t) (\text{rot } D\mathbf{z}(t), \mathbf{w}(t))_{\mathbf{L}^2(0,L)} dt + \frac{\vartheta}{2} \int_0^T \langle |\nabla\phi|^2 \circ \mathbf{z}(t) \text{rot } D\mathbf{z}(t), \mathbf{w}(t) \rangle dt \\ & - \int_0^T \langle |D\mathbf{z}(t)| \varphi_{\mathbf{z}} \circ \mathbf{z}(t), \mathbf{w}(t) \rangle dt + \int_0^T \lambda(t) \langle \delta Q(\mathbf{z}(t)), \mathbf{w}(t) \rangle dt \\ & + \int_0^T \mu(t) Q(\mathbf{z}(t)) dt = \int_0^T \mu(t) c(t) dt + (\boldsymbol{\chi}_1, \mathbf{w}(0))_{\mathbf{L}^2(0,L)}, \end{aligned} \quad (2.26a)$$

where the semilinear form $a_s : \mathbf{H}^2(0, L) \times \mathbf{H}^2(0, L) \rightarrow \mathbb{R}$ is defined by

$$a_s(\mathbf{z}; \mathbf{w}) = ((1 - |D\mathbf{z}|^{-1})D\mathbf{z}, D\mathbf{w})_{\mathbf{L}^2(0,L)} + \epsilon(D^2\mathbf{z}, D^2\mathbf{w})_{\mathbf{L}^2(0,L)} \quad (2.26b)$$

and $\langle \cdot, \cdot \rangle$ denotes the duality pairing between $\mathbf{H}^{-2}(0, L)$ and $\mathbf{H}_0^2(0, L)$. Moreover, $\delta Q : \mathbf{H}^2(0, L) \rightarrow \mathbf{H}^{-2}(0, L)$ denotes the Fréchet derivative of the volume functional Q .

In the weak formulation (2.26a), the pressure level p_0 can be identified with the Lagrange multiplier $\lambda \in L^2(0, T)$. More precisely, if we denote by $(\mathbf{z}, \lambda)^0$ the solution to (2.26a) for $p_0 = 0$ and by $(\mathbf{z}, \lambda)^1$ the solution to (2.26a) for some arbitrary $p_0 \in L^2(0, T)$, then it holds that $\mathbf{z}^1 = \mathbf{z}^0$ and $\lambda^1 = \lambda^0 + p_0$. To prove this assertion, we will show that

$$\langle \delta Q(\mathbf{z}(t)), \mathbf{w}(t) \rangle = (\text{rot } D\mathbf{z}(t), \mathbf{w}(t))_{\mathbf{L}^2(0,L)}, \quad (2.27)$$

for all admissible structure configurations $\mathbf{z} \in \boldsymbol{\chi}_0 + W_0(0, T)$ and all $\mathbf{w} \in L^2(0, T; \mathbf{H}_0^2(0, L))$. The time-dependence of the structure configuration is in fact irrelevant in (2.27) and will be suppressed in the ensuing derivation. We first note that

$$Q(\mathbf{z}) = \int_{\Omega_t} d\mathbf{x} = \frac{1}{2} \int_{\Omega_t} \text{div } \mathbf{x} d\mathbf{x} = \frac{1}{2} \oint_{\partial\Omega_t} \mathbf{x} \cdot \mathbf{n} d\sigma_t = \frac{1}{2} \int_0^\Lambda \mathbf{z}(s) \cdot \text{rot } D\mathbf{z}(s) ds. \quad (2.28)$$

The penultimate expression in (2.28) is a straightforward consequence of the divergence theorem. The ultimate expression follows from the transformation $s \mapsto \mathbf{x} = \mathbf{z}(s)$. We consider an arbitrary $\mathbf{w} \in \mathbf{H}_0^2(0, L)$ and extend it to (L, Λ) by zero. The extension is still denoted by \mathbf{w} . From (2.28), we obtain:

$$\langle \delta Q(\mathbf{z}), \mathbf{w} \rangle := \frac{d}{d\epsilon} Q(\mathbf{z} + \epsilon\mathbf{w}) \Big|_{\epsilon=0} = \frac{1}{2} (\text{rot } D\mathbf{z}, \mathbf{w})_{\mathbf{L}^2(0,L)} + \frac{1}{2} (\mathbf{z}, \text{rot } D\mathbf{w})_{\mathbf{L}^2(0,L)}. \quad (2.29)$$

It is easily verified that the right member of (2.29) is linear in \mathbf{z} and \mathbf{w} and that

$$\left| \frac{1}{2} (\text{rot } D\mathbf{z}, \mathbf{w})_{\mathbf{L}^2(0,L)} + \frac{1}{2} (\mathbf{z}, \text{rot } D\mathbf{w})_{\mathbf{L}^2(0,L)} \right| \leq \|\mathbf{z}\|_{\mathbf{H}^2(0,L)} \|\mathbf{w}\|_{\mathbf{H}^2(0,L)}. \quad (2.30)$$

Hence, the Fréchet derivative $\delta Q(\cdot)$ can be identified with a linear continuous operator from $\mathbf{H}^2(0, L)$ into $\mathbf{H}^{-2}(0, L)$, and for each $\mathbf{z} \in \mathbf{H}^2(0, L)$ the duality pairing of $\delta Q(\mathbf{z})$ with $\mathbf{w} \in \mathbf{H}_0^2(0, L)$ is defined by the right member of (2.29). The identity (2.27) is obtained by recasting the second term in the right member of (2.29) into:

$$(\mathbf{z}, \text{rot } D\mathbf{w})_{\mathbf{L}^2(0,L)} = -(\text{rot } \mathbf{z}, D\mathbf{w})_{\mathbf{L}^2(0,L)} = (\text{rot } D\mathbf{z}, \mathbf{w})_{\mathbf{L}^2(0,L)}. \quad (2.31)$$

The first identity in (2.31) is a consequence of the skew-symmetry of the rotation operator. The second identity follows from integration-by-parts and $\mathbf{w}|_{\{0,L\}} = 0$.

2.5 Contact forces

In the treatment of complex folded geometries, adequate modeling of self-contact of the membrane is imperative to avoid self-intersection. Because our primary interest concerns the coupled problem described in §§2.1-4 and, in this context, contact modeling is only accessory, we shall be contented with any cogent contact model that prevents self-intersection. For this reason, we shall consider a soft-contact model based on repulsive potentials, instead of a hard-contact model, as the latter requires contact detection, which is nontrivial. Moreover, the soft-contact model admits an efficient implementation by recycling the kernels that have already been generated in the boundary-element method for the fluid subproblem.

In the soft-contact model, each segment of the membrane exerts a force on every other segment, depending on their relative distance and orientation. We model the contact-induced traction on the structure, $\mathbf{z} \mapsto \boldsymbol{\varphi}_{\mathbf{z}}$, as the marginal of a vector-valued traction density, i.e., we postulate:

$$\boldsymbol{\varphi}_{\mathbf{z}}(\mathbf{x}) = \zeta \oint_{\partial\Omega} \mathbf{F}(\mathbf{x}, \mathbf{y}) d\sigma(\mathbf{y}), \quad (2.32)$$

for some traction density $\mathbf{F} : \partial\Omega \times \partial\Omega \rightarrow \mathbb{R}^2$, with $\zeta > 0$ a model parameter. Let us note that $\boldsymbol{\varphi}_{\mathbf{z}}$ depends implicitly on the structure configuration, \mathbf{z} , on account of the dependence of the domain Ω on \mathbf{z} . Moreover, we assume that the inflow boundary Γ_{in} also exerts a contact traction. The time dependence of the structural configuration and of the domain are irrelevant for the exposition, and will be suppressed. The traction density should comply with the following elementary conditions:

- C1. The traction density should be essentially local, i.e., it should have local support or decay rapidly as the distance $|\mathbf{x} - \mathbf{y}|$ increases;
- C2. The traction density is repulsive and acts in the direction $\mathbf{x} - \mathbf{y}$ of the relative position of segments of the membrane;
- C3. The traction at any point induced by segments in the vicinity of that point vanishes. This means that for each $\mathbf{x} \in \partial\Omega$ and each $\varepsilon > 0$ there exist a $\delta > 0$ and a connected subset $\Gamma_\delta \subset \partial\Omega$ such that $\mathbf{x} \in \Gamma_\delta$ and

$$\frac{1}{\text{meas}\Gamma_\delta} \left| \int_{\Gamma_\delta} \mathbf{F}(\mathbf{x}, \mathbf{y}) d\sigma(\mathbf{y}) \right| < \varepsilon \quad (2.33)$$

with $\text{meas}\Gamma_\delta$ the surface measure of Γ_δ ;

- C4. The contact force should prevent self-intersection of the membrane. To this end, the traction density must approach infinity if $\mathbf{y} \rightarrow \mathbf{x}$ while \mathbf{y} and \mathbf{x} are separated on the membrane. In particular, if there exists a sequence $\{\mathbf{y}_n\} \subset \Gamma$, $\mathbf{y}_n \rightarrow \mathbf{x}$ as $n \rightarrow \infty$, a corresponding sequence of sections $\Gamma_n \subset \Gamma$,

$$\Gamma_n = \{\Gamma_n \text{ is the smallest connected subset of } \partial\Omega \text{ containing } \mathbf{x} \text{ and } \mathbf{y}\} \quad (2.34)$$

and a number $\varepsilon > 0$ such that $\text{meas}\Gamma_n \geq \varepsilon$ as $n \rightarrow \infty$, then $|\mathbf{F}(\mathbf{x}, \mathbf{y}_n)| \rightarrow \infty$ as $n \rightarrow \infty$; cf. also condition C3;

- C5. The traction density should satisfy a reciprocity principle in accordance with Newton's third law of motion, which implies $\mathbf{F}(\mathbf{y}, \mathbf{x}) = -\mathbf{F}(\mathbf{x}, \mathbf{y})$.

An important observation pertains to the fact that, in the finite-element approximation, the concomitant computational complexity of the soft-contact model is proportional to the number of elements squared, as for each element we have to visit all other elements to determine the relative distances. In the present setting, however, the relative distances have already been computed in the boundary-integral formulation of the fluid subproblem. Moreover, we will show that the dependence of the

contact force on the relative distance and orientation can be formulated such that the aforementioned conditions are obeyed, and that the traction density can be composed of the singular kernel in the double-layer potential in (2.4b). The authors are not aware of previous work on such recycling of discrete kernels of a boundary-integral formulation to determine contact forces.

To facilitate the presentation, we factorize the traction density in four components according to $\mathbf{F}(\mathbf{x}, \mathbf{y}) = b(r/d) \nu(\mathbf{x}, \mathbf{y}) r^{-1} \mathbf{d}(\mathbf{x}, \mathbf{y})$, where $r := |\mathbf{x} - \mathbf{y}|$ is a condensed notation for the distance between \mathbf{x} and \mathbf{y} and $d > 0$ is a preselected cut-off radius. The function b serves to localize the traction density in accordance with condition C1. To this end, we apply a smooth window function based on a b-spline $b : \mathbb{R}_+ \rightarrow [0, 1]$:

$$b(r) := \begin{cases} 1 - 3r^2, & r < 1/3, \\ 3/2 - 3r + (3/2)r^2, & 1/3 \leq r \leq 1, \\ 0, & \text{otherwise,} \end{cases}$$

Let us remark that this is a common kernel in the realm of smooth particle hydrodynamics. The vector-valued function \mathbf{d} accounts for the directional dependence in condition C2:

$$\mathbf{d}(\mathbf{x}, \mathbf{y}) = r^{-1}(\mathbf{x} - \mathbf{y}).$$

The function ν serves to impose the non-contiguity condition C3 and the reciprocity principle C5:

$$\nu(\mathbf{x}, \mathbf{y}) = \left| r^{-1}(\mathbf{x} - \mathbf{y}) \cdot (\mathbf{n}(\mathbf{x}) - \mathbf{n}(\mathbf{y})) \right|. \quad (2.35)$$

Finally, the factor r^{-1} serves to introduce the singular behavior of the traction density to fulfill condition C4. Another important argument for selecting the particular form of ν in (2.35) and the r^{-1} dependence, is that these lead to a traction density that can be conveniently expressed in terms of the singular kernel $\partial_{\mathbf{n}} G$ according to (2.6) in the double-layer potential.

The expression for ν in (2.35) warrants some further elaboration. To prove that the corresponding traction density satisfies condition C3, we consider a parametrization $(0, L) \ni s \mapsto \mathbf{z}(s) \in \Gamma$, and we note that for $|\alpha| < \delta$ and $\delta \rightarrow +0$, it holds that

$$\begin{aligned} & \mathbf{F}(\mathbf{z}(s), \mathbf{z}(s + \alpha)) \\ &= b\left(\frac{|\mathbf{z}(s) - \mathbf{z}(s + \alpha)|}{d}\right) \left| \frac{\mathbf{z}(s) - \mathbf{z}(s + \alpha)}{|\mathbf{z}(s) - \mathbf{z}(s + \alpha)|^3} \cdot \left(\frac{\text{rot} D\mathbf{z}(s)}{|D\mathbf{z}(s)|} - \frac{\text{rot} D\mathbf{z}(s + \alpha)}{|D\mathbf{z}(s + \alpha)|} \right) \right| (\mathbf{z}(s) - \mathbf{z}(s + \alpha)) \\ &= b\left(\frac{|D\mathbf{z}(s)\alpha + o(\delta)|}{d}\right) \left| \frac{-D\mathbf{z}(s)\alpha + o(\delta)}{|D\mathbf{z}(s)\alpha + o(\delta)|^3} \cdot \left(\frac{D\mathbf{z}(s) \cdot D^2\mathbf{z}(s) \text{rot} D\mathbf{z}(s)\alpha}{|D\mathbf{z}(s)|^3} - \frac{\text{rot} D^2\mathbf{z}(s)\alpha}{|D\mathbf{z}(s)|} + o(\delta) \right) \right| \\ & \quad \times (-D\mathbf{z}(s)\alpha + o(\delta)) \\ &= \mathbf{C}_{\mathbf{z}(s)} \frac{\alpha}{|\alpha|} + o(1) \end{aligned} \quad (2.36)$$

where $o(\cdot)$ denotes the Landau symbol with the property that $o(\delta^\beta)/|\delta^\beta| \rightarrow 0$ as $\delta \rightarrow 0$ for all $\beta \geq 0$ and

$$\mathbf{C}_{\mathbf{z}(s)} = - \left| \frac{D\mathbf{z}(s)}{|D\mathbf{z}(s)|} \cdot \left(\frac{D\mathbf{z}(s) \cdot D^2\mathbf{z}(s) \text{rot} D\mathbf{z}(s)}{|D\mathbf{z}(s)|^3} - \frac{\text{rot} D^2\mathbf{z}(s)}{|D\mathbf{z}(s)|} \right) \right| D\mathbf{z}(s)$$

supposing that all the above derivatives exist. Hence, the leading order term of $\mathbf{F}(\mathbf{z}(s), \mathbf{z}(s + \alpha))$ corresponds to an odd function in α , and its integral on a symmetric interval around $\alpha = 0$ vanishes. More precisely, selecting Γ_δ in (2.33) according to

$$\Gamma_\delta = \{\mathbf{x} \in \Gamma : \mathbf{x} = \mathbf{z}(s + \alpha), |\alpha| < \delta\} \quad (2.37)$$

we obtain, in the limit $\delta \rightarrow +0$,

$$\begin{aligned} \frac{1}{\text{meas } \Gamma_\delta} \left| \int_{\Gamma_\delta} \mathbf{F}(z(s), \mathbf{y}) d\sigma(\mathbf{y}) \right| \\ = \frac{1}{2\delta |Dz(s)| + o(\delta)} \left| \int_{-\delta}^{\delta} \left(\mathbf{C}_z(s) \frac{\alpha}{|\alpha|} + o(1) \right) |Dz(s) + o(1)| d\alpha \right| = o(1), \end{aligned} \quad (2.38)$$

and, hence, for each $\varepsilon > 0$ there exists a $\delta > 0$ such that (2.33) holds with $\mathbf{x} = z(s)$.

Summarizing, the contact-induced traction on the structure reads:

$$\begin{aligned} \varphi_z(\mathbf{x}) &:= \zeta \oint_{\partial\Omega} \mathbf{F}(\mathbf{x}, \mathbf{y}) d\sigma(\mathbf{y}) = 2\zeta \oint_{\partial\Omega} b(\mathbf{x}, \mathbf{y}) \left| \frac{(\mathbf{x} - \mathbf{y}) \cdot (\mathbf{n}(\mathbf{x}) - \mathbf{n}(\mathbf{y}))}{2r^2} \right| \frac{\mathbf{x} - \mathbf{y}}{r} d\sigma(\mathbf{y}) \\ &= 2\pi\zeta \oint_{\partial\Omega} b(\mathbf{x}, \mathbf{y}) |\partial_n G(\mathbf{x}, \mathbf{y}) + \partial_n G(\mathbf{y}, \mathbf{x})| \frac{\mathbf{x} - \mathbf{y}}{r} d\sigma(\mathbf{y}). \end{aligned} \quad (2.39)$$

In a numerical procedure, the expression $\varphi_z(\mathbf{x})$ is required at certain integration points, $\{\mathbf{x}_i\}$. Moreover, for each $\mathbf{x} \in \{\mathbf{x}_i\}$, the integral on $\partial\Omega$ in (2.39) is computed by means of a quadrature rule, which involves determining the value of the integrand at points $\{\mathbf{y}_j\}$. Hence, the value of the integrand is required for all pairs of points $(\mathbf{x}, \mathbf{y}) \in \{\mathbf{x}_i\} \times \{\mathbf{y}_j\}$. The final expression in (2.39) conveys that φ_z can indeed be efficiently computed, because the values of the singular kernel $\partial_n G(\mathbf{x}, \mathbf{y})$ and of the relative positions $\mathbf{x} - \mathbf{y}$ at $\{\mathbf{x}_i\} \times \{\mathbf{y}_j\}$ have already been computed in the numerical approximation of the double-layer potential (2.4b).

To establish that the contact-induced traction defines a meaningful load on the structure, we must show that the map:

$$\mathbf{w} \mapsto \int_0^T \int_0^L \mathbf{w}(t, s) \cdot \varphi_z \circ z(t, s) |Dz(t, s)| ds dt \quad (2.40)$$

defines a continuous linear functional on $L^2(0, T; \mathbf{H}_0^2(0, L))$; cf. (2.16) and (2.22). We first note that by Hölder's inequality, we have

$$\begin{aligned} \left| \int_0^T \int_0^L \mathbf{w}(t, s) \cdot \varphi_z \circ z(t, s) |Dz(t, s)| ds dt \right| \\ \leq \|\mathbf{w}\|_{L^2(0, T; \mathbf{L}^\infty(0, L))} \|Dz\|_{L^\infty(0, T; \mathbf{L}^\infty(0, L))} \|\varphi_z \circ z\|_{L^2(0, T; \mathbf{L}^1(0, L))} \end{aligned} \quad (2.41)$$

Hence, by the same arguments as in Section 2.3, it remains to bound the right-most factor in (2.41). The function $\varphi_z \circ z(t, s)$ can be expanded into:

$$\begin{aligned} \varphi_z \circ z(t, s) &= \zeta \oint_{\partial\Omega} \mathbf{F}(z(t, s), \mathbf{y}) d\sigma_t(\mathbf{y}) \\ &= 2\pi\zeta \oint_{\partial\Omega} \left(-\partial_n G(z(t, s), \mathbf{y}) - \partial_n G(\mathbf{y}, z(t, s)) \right) \Theta(z(t, s), \mathbf{y}) d\sigma_t(\mathbf{y}) \end{aligned} \quad (2.42)$$

where

$$\Theta(\mathbf{x}, \mathbf{y}) = b \left(\frac{|\mathbf{x} - \mathbf{y}|}{d} \right) \mathbb{1}_{\text{supp}(\nu)}(\mathbf{x}, \mathbf{y}) \frac{\mathbf{x} - \mathbf{y}}{|\mathbf{x} - \mathbf{y}|} \quad (2.43)$$

with $\mathbb{1}_{\text{supp}(\nu)}$ the characteristic function of the support of ν according to (2.35), i.e., $\mathbb{1}_{\text{supp}(\nu)}(\mathbf{x}, \mathbf{y})$ is 1 if $\nu(\mathbf{x}, \mathbf{y}) \neq 0$ and 0 otherwise. Because Θ in the ultimate expression depends on \mathbf{z} , we cannot rely on standard results on continuity of the double-layer potential and its adjoint to bound the right-most factor in (2.41). A detailed analysis of $\varphi_z \circ z(t, s)$ is technical and is beyond the scope of this paper, and boundedness of $\|\varphi_z \circ z\|_{L^2(0, T; \mathbf{L}^1(0, L))}$ is left as a conjecture. However, in support of this conjecture, we note that the asymptotic result in (2.36) implies that, under suitable smoothness conditions on \mathbf{z} , the traction density $\mathbf{F}(z(s), z(s + \alpha))$ is bounded at the singularity of $\partial_n G$, i.e., in the limit as $\alpha \rightarrow 0$.

3. Numerical approximation and solution

In this section, we consider the numerical approximation of the aggregated fluid-structure-interaction problem, composed of the weak form of the boundary-integral formulation of the fluid equations (2.7), the weak formulation of the membrane equations and the compatibility condition (2.26), and the kinematic and dynamic transmission conditions (2.19) and (2.20). Section 3.1 presents the spatial and temporal discretizations of the fluid and structure subproblems. The aggregated system is solved by means of a partitioned iterative solution procedure, which is elaborated in Section 3.2.

3.1 Finite-element approximations

Recalling that the initial wet boundary Γ_0 and the inflow boundary Γ_{in} of the fluid domain are parametrized with respect to the arc-length intervals $(0, L)$ and (L, Λ) , we introduce a sequence of nested regular partitions \mathcal{S}^h of these intervals, parametrized by a strictly decreasing sequence of mesh parameters $h \in \{h_0, h_1, \dots\}$. For each h , the partition \mathcal{S}^h provides a cover of $(0, L)$ and (L, Λ) by disjoint open subsets $\{\kappa_1^h, \kappa_2^h, \dots\}$. The regularity of the partitions implies that there exist moderate constants \underline{c} and \bar{c} , independent of h , such that for each $\kappa \in \mathcal{S}^h$ it holds that $\underline{c}h \leq \text{meas}\kappa \leq \bar{c}h$. The nesting of the partitions implies that whenever $h_1 < h_0$, for each subset $\kappa \in \mathcal{S}^{h_1}$ there exists a subset $\varkappa \in \mathcal{S}^{h_0}$ such that $\kappa \subseteq \varkappa$. A partition \mathcal{S}^h and the subintervals it contains are referred to as a *mesh* and *elements*, respectively.

The partitions form the substructure of the finite-element approximation spaces for the fluid and structure subproblems,

$$\mathbb{S}^h := \{z \in C^1(0, L) : z|_{\kappa} \in \mathbb{P}^3(\kappa, \mathbb{R}^2) \forall \kappa \in \mathcal{S}^h, \kappa \subset (0, L)\}, \quad (3.1a)$$

$$\mathbb{F}_p^h := \{\phi \in C^0(0, \Lambda) : \phi|_{\kappa} \in \mathbb{P}^1(\kappa, \mathbb{R}) \forall \kappa \in \mathcal{S}^h; \phi(0) = \phi(\Lambda)\}, \quad (3.1b)$$

respectively, where $\mathbb{P}^p(\kappa, \mathbb{R}^n)$ represents the class of polynomials of degree $\leq p$ from κ into \mathbb{R}^n . The approximation space $\mathbb{S}^h \subset \mathbf{H}^2(0, L)$ (resp. $\mathbb{F}_p^h \subset H_p^1(0, \Lambda)$, viz., the periodic functions in $H^1(0, \Lambda)$) is $\mathbf{H}^2(0, L)$ -conforming (resp. $H_p^1(0, \Lambda)$ conforming). On account of the regularity and nesting properties of the meshes, the sequence of approximation spaces \mathbb{S}^h is nested and asymptotically in $\mathbf{H}^2(0, L)$, i.e., $\mathbb{S}^{h_0} \subset \mathbb{S}_1^h \subset \dots \subseteq \mathbf{H}^2(0, L)$ and $\mathbb{S}^h \rightarrow \mathbf{H}^2(0, L)$ as $h \rightarrow 0$. Similarly, \mathbb{F}_p^h is a sequence of asymptotically dense nested subspaces in $H_p^1(0, \Lambda)$.

To facilitate the evaluation of the singular integrals in the boundary-element formulation of the fluid, we do not use the element-wise polynomial representation of the boundary provided by the approximation of the structure position but, instead, we select a continuous element-wise linear approximation of the domain boundary, which nodally coincides with the structure position or, along the section associated with the inflow boundary, with the initial configuration. In particular, for an approximate structural position $z^h \in \mathcal{S}^h$, the boundary of the approximate fluid domain is parametrized according to $\partial\Omega^h = \{x \in \mathbb{R}^2 : x = \tilde{z}^h(s), s \in (0, \Lambda)\}$, where \tilde{z}^h is the unique function defined by:

$$\begin{aligned} \{\tilde{z}^h \in C^0(0, \Lambda) : \tilde{z}^h|_{\kappa} \in \mathbb{P}^1(\kappa, \mathbb{R}^2) \forall \kappa \in \mathcal{S}^h; \tilde{z}^h(0) = \chi_0(0); \tilde{z}^h(L) = \chi_0(L); \\ \tilde{z}^h(\Lambda) = \chi_0(0); \tilde{z}^h|_{\mathcal{N}^h \cap (0, L)} = z^h|_{\mathcal{N}^h \cap (0, L)}; \tilde{z}^h|_{\mathcal{N}^h \cap (L, \Lambda)} = \chi_0|_{\mathcal{N}^h \cap (L, \Lambda)}\}, \end{aligned} \quad (3.2)$$

where $\mathcal{N}^h := \{\partial\kappa; \kappa \in \mathcal{S}^h\}$ (without repetitions) is the set of nodes corresponding to \mathcal{S}^h . Singular contributions to the integrals in (2.7) occur on elements where both ψ and ϕ are supported. Denote the linear basis on $\tilde{z}^h(\kappa)$ by N_i^{κ} , $i \in \{0, 1\}$. For convenience of notation we introduce $J_{\kappa} := |D\tilde{z}^h|_{\kappa}| \text{meas } \kappa$ which is a constant on κ by virtue of the approximation \tilde{z}^h of the configuration. We can then compute the singular contributions by combinations of the integrals

$$\begin{aligned} (N_i, KN_j)_{L^2(\tilde{z}^h(\kappa))} &= 0, \\ (N_i, VN_j)_{L^2(\tilde{z}^h(\kappa))} &= (6 + (-1)^{i+j} - 4 \log J_{\kappa}) \frac{J_{\kappa}^2}{2\pi}. \end{aligned}$$

For the temporal discretization of the structure equation (2.26), we apply an implicit backward-Euler approximation. To facilitate the formulation of the discretization of the fluid-structure-interaction problem, we denote by $\mathbf{z}_0^h \in \mathbb{S}^h$ a suitable approximation to the initial position $\boldsymbol{\chi}_0$ such that $\mathbf{z}_0^h|_{\{0,L\}} = \boldsymbol{\chi}_0|_{\{0,L\}}$, and by $\mathbb{S}_0^h = \{\mathbf{z}^h \in \mathbb{S}^h : \mathbf{z}|_{\{0,L\}} = 0\}$ the functions in \mathbb{S}^h that vanish at the end points of the interval $(0, L)$. The discrete approximation of the aggregated fluid-structure-interaction problem can then be formulated as: *For $n = 1, 2, \dots$, find $(\mathbf{z}_n^h, \lambda_n, \phi_n^h, \zeta_n) \in (\mathbf{z}_0^h + \mathbb{S}_0^h) \times \mathbb{R} \times \mathbb{F}_p^h \times \mathbb{R}$, such that for all $(\mathbf{w}, \mu, \psi, v) \in \mathbb{S}_0^h \times \mathbb{R} \times \mathbb{F}_p^h \times \mathbb{R}$, there holds:*

$$\begin{aligned} & \tau^{-2}(\mathbf{z}_n^h, \mathbf{w})_{L^2(0,L)} + a_s(\mathbf{z}_n^h; \mathbf{w}) - \lambda_n(\text{rot } D\mathbf{z}_n^h, \mathbf{w})_{L^2(0,L)} + \frac{\vartheta}{2} \left(|\nabla_\Gamma \phi_n^h|^2 \circ \tilde{\mathbf{z}}_n^h \text{rot } D\mathbf{z}_n^h, \mathbf{w} \right)_{L^2(0,L)} \\ & + \frac{\vartheta}{2} \left((\tau^{-1}(\mathbf{z}_n^h - \mathbf{z}_{n-1}^h) \cdot (|D\mathbf{z}_n^h|^{-1} \text{rot } D\mathbf{z}_n^h))^2 \text{rot } D\mathbf{z}_n^h, \mathbf{w} \right)_{L^2(0,L)} - (|D\mathbf{z}_n^h| \mathbf{F}_{\mathbf{z}_n^h} \circ \mathbf{z}_n^h, \mathbf{w})_{L^2(0,L)} \\ & + \mu Q(\mathbf{z}_n^h) + (\frac{1}{2} \phi_n^h + K \phi_n^h, \psi)_{L^2(\partial\Omega_n^h)} - \left(V(|D\tilde{\mathbf{z}}_n^h|^{-1} \text{rot } D\tilde{\mathbf{z}}_n^h \cdot (\tau^{-1}(\tilde{\mathbf{z}}_n^h - \tilde{\mathbf{z}}_{n-1}^h)) \circ (\tilde{\mathbf{z}}_n^h)^{-1}, \psi) \right)_{L^2(\Gamma_n^h)} \\ & + v(\phi_n^h, 1)_{L^2(\partial\Omega_n^h)} + \zeta_n(\psi, 1)_{L^2(\partial\Omega_n^h)} = \tau^{-2}(\mathbf{z}_{n-1}^h, \mathbf{w})_{L^2(0,L)} + \tau^{-1}(\mathbf{v}_{n-1}^h, \mathbf{w})_{L^2(0,L)} + \mu c(t_n) + (Vq, \psi)_{L^2(\Gamma_{in}^h)} \end{aligned} \quad (3.3)$$

with τ the time step and $t_n = n\tau$. Furthermore, \mathbf{v}_0^h denotes a suitable approximation of the initial velocity and $\mathbf{v}_n^h = \tau^{-1}(\mathbf{z}_n^h - \mathbf{z}_{n-1}^h)$ for $n = 1, 2, \dots$; cf. (2.26) and (2.7). It is to be noted that the term pertaining to the pressure level p_0 in (2.26) has been merged with the Lagrange-multiplier term, in accordance with the exposition in Section 2.4. Moreover, in (3.3), the $|\nabla\phi|^2$ term in (2.26) has been expanded in accordance with the ultimate identity in (2.20), and the orthogonality conditions $(\phi, 1)_{L^2(\partial\Omega_t)} = 0$ and $(\psi, 1)_{L^2(\partial\Omega_t)} = 0$ in (2.7) are instead imposed by means of Lagrange multipliers.

3.2 Partitioned solution of coupled system

Having fixed solution methods for both the fluid and structure subsystems, we elaborate the partitioned solution of the coupled system, shown in table 1. A linear extrapolation of the initial data serves as a first approximation of the new coupled solution. Within a fluid-structure subcycle, a structural solve is performed first, to ensure compatibility of the fluid boundary data. The subcycle is considered converged if the norm of the structure residual is below the tolerance before a Newton solve is performed. In performing Newton iterations, the pressure and contact loads are treated explicitly whereas the stiffness semilinear form and volume constraint are consistently linearized as

$$\langle \delta a_s(\mathbf{z}_n^h; \mathbf{w}), \delta \mathbf{z} \rangle = \left([(1 - |D\mathbf{z}_n^h|^{-1}) \text{Id} + |D\mathbf{z}_n^h|^{-3} D\mathbf{z}_n^h \otimes \mathbf{z}_n^h] D\delta \mathbf{z}, D\mathbf{w} \right)_{L^2(0,L)} + \epsilon(\delta \mathbf{z}, \mathbf{w})_{\mathbf{H}_{\text{sem}}^2(0,L)}$$

and

$$\langle \delta(\delta Q(\mathbf{z}_n^h), \mathbf{w}), \delta \mathbf{z}_n^h \rangle = (\text{rot } D\delta \mathbf{z}, \mathbf{w})_{L^2(0,L)}$$

respectively.

The return statement is not reached if either the coupling iteration or the structure solve does not converge due to, for instance, large contact forces. This high temporary stiffness of the problem is resolved by invoking the simplest possible time adaptivity, where the time step is resolved with increasingly finer time steps $2^{-k}\tau$ until the iterations converge. At the subsequent time level, k is redefined according to $k = \max(k - 1, 0)$.

Though performing a linearization on the aggregate fluid-structure system is known to improve convergence of the discrete coupled problem, the complexity rises considerably. The \mathbf{z}_n^h -derivative of the fluid subproblem is highly nontrivial due to the \mathbf{z}_n^h -dependence of the kernels. For this reason, a partitioned solution strategy was preferred above a monolithic scheme.

4. Numerical examples

To demonstrate the performance of the FE/BE approach proposed here, we first perform a convergence study on the case of a pancake-shaped domain, adapted from [6, 30], see section 4.1. Secondly, we

Table 1: Partitioned solution algorithm in Python™ pseudo code, given numerical parameters (τ , imax , jmax , TOL), and input ($\mathbf{z}_t, \mathbf{z}_{t-\tau}, \phi_t, q, c_t$). For simplicity, we have incorporated the Lagrange multipliers into the respective solution vectors. Note that indices do not denote tensor entries, but iterates.

```

 $\mathbf{z}_{00}, \phi_0 = \text{extrapolate}( \tau, \mathbf{z}_t, \mathbf{z}_{t-\tau}, \phi_t )$ 

# Coupling iteration
for  $0 \leq i < \text{imax}$ :

    # Structure solve
    for  $0 \leq j < \text{jmax}$ :
         $r_{ij} = \text{assembleResidual}( \mathbf{z}_{ij}, \mathbf{z}_t, \phi_i, c_t, q, \tau )$ 
        if  $\|r_{ij}\|_{L^2} < \text{TOL}$ : break
         $(\delta r)_{ij} = \text{assembleTangent}( \mathbf{z}_{ij} )$ 
         $\mathbf{z}_{ij+1} = [\delta r]_{ij}^{-1} r_{ij}$ 

    # Return statement
    if not j: return  $\mathbf{z}_{ij}$ 

# Fluid solve
 $Vh_i, K_i = \text{assembleFluid}( \mathbf{z}_{ij}, \mathbf{z}_t )$ 
 $\phi_{i+1} = [1/2 + K_i]^{-1} Vh_i$ 

```

consider a simple folded configuration to observe the response and convergence rates in the presence of contact forces. Let us note that the derivation of convergence rates for coupled problems is very technical, see for instance [16]. In the exposition below, we restrict ourselves to the experimentally observed convergence rates.

4.1 Pancake-shaped domain

The initial configuration, χ_0 , is as given in figure 2 with geometrical parameters $r = 1/3, w = 4$. Furthermore we set the mass ratio ϑ to 0.1, and perform spatial and temporal convergence tests with regularization set to $\epsilon = 1 \times 10^{-4}$. The parametric domain is divided into elements of size $h \in L/\{24, 48, 72, 96, 144, 288\}$. The time domain $(0, T)$ is divided into increments of $\tau \in \text{per}/2^{\{5, \dots, 10\}}$ with $\text{per} = (\Lambda/\pi)^2$ an approximation of the period of the first eigenmotion (based on the flexural term). Finally, the inflow is specified as $q = \bar{q}\sigma(s - L)\theta(t)$, with

$$\sigma(s) = 4s(r - s)/r^2,$$

$$\theta(t) = \frac{1}{t_2} \begin{cases} (1 - \cos(\pi t/t_1))/2, & 0 < t \leq t_1, \\ 1, & t_1 < t \leq t_2, \\ (1 + \cos(\pi(t - t_2)/t_1))/2, & t_2 < t \leq t_1 + t_2, \\ 0, & t_1 + t_2 < t. \end{cases}$$

In these relations we have $t_1 = 100, t_2 = 2t_1, T = 4t_1$ and the mean influx $\bar{q} = (|\Omega(0)| - |\Omega_t|)/t_2$. The initial volume can be found in terms of w and r ⁱ and the final volume is specified as $|\Omega_t| = 1.05\Lambda^2/4\pi$. Note that the mean flux has a negative sign as it is directed into the enclosure.

ⁱWe have $|\Omega(0)| = 2wr - r^2 + \pi r^2/2$.

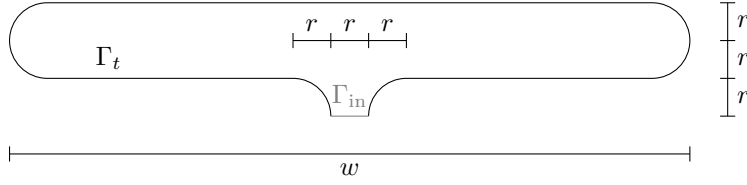
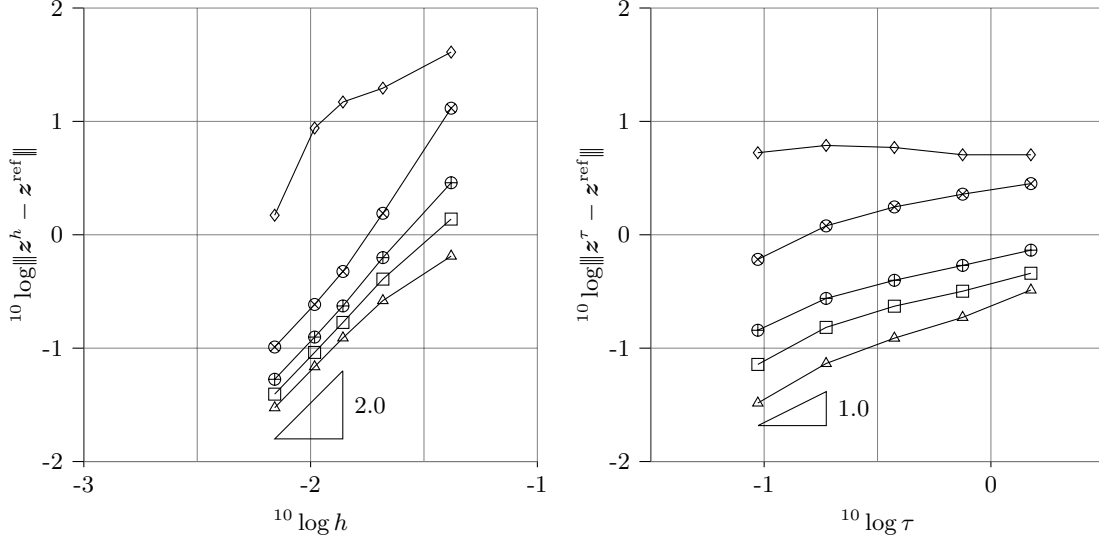


Figure 2: Pancake-shaped domain, initial geometry.

Figure 3: Convergence behavior in the space-time norm with symbols $\{\triangle, \square, \oplus, \otimes, \diamond\}$ representing time levels $t = \{0.750, 3.00, 12.0, 192, 400\}$, respectively.

The convergence behavior is assessed in the space-time norm of the structure defined by

$$\|\mathbf{z}\| := \|\mathbf{z}\|_{L^2(0,T;\mathbf{H}^2(0,L))} = \left(\int_0^T \int_0^L \sum_{\alpha \leq 2} |D^\alpha \mathbf{z}|^2 ds dt \right)^{1/2} \quad (4.1)$$

and is plotted in figure 3, with reference solution \mathbf{z}^{ref} obtained from the finest discretization in space and time. Spatial convergence is given in the left panel. The optimal (quadratic) convergence rate of the decoupled structural problem seems to be preserved in the initial response. This trend breaks down when simulation times increase and phase-lag dominates the errors. This is due to the fact that, on long time intervals, marginal phase differences cause large deviations in the norm.

For temporal convergence (right panel) the linear rate expected of the backward Euler scheme is retained. Also, a linear increase in time of the error norm is observed initially, just like in the spatial convergence case. A reduction in the convergence rate is observed as the time interval increases because the phase-lag precludes correlation between the different time-steps. It is however anticipated that even for long time intervals, the asymptotic first-order convergence is recovered at very small time steps.

Snapshots at different time-levels are given in figure 4. The initial inflation process is quasi-static. When the airbag is fully inflated, the momentum build-up in the fluid due to the influx causes an upward movement of the airbag. At this point the compressive force at the top of the airbag is seen to cause wrinkling, which is smoothed out by the flexural regularization. The upward movement

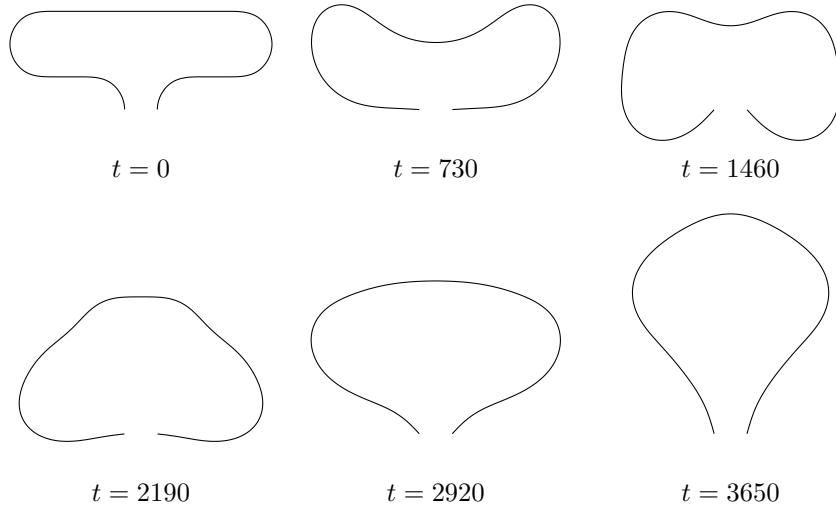


Figure 4: Snapshots of the pancake response, for $w = 4$, colors indicate the static pressure.

is subsequently absorbed by the hinged supports, sending waves through the structure. These waves in the structural response are seen to be accompanied by pressure minima. A periodic bounding motion sets in, called the airbag breathing motion. The mathematical system is conservative, however, numerical dissipation causes this motion to diminish and the displacement to tend to an equilibrium solution, the circle. Observe the very large deformations of the domain, for which a significant number of remeshing cycles would be necessary in an ALE-type approach.

In the above pancake case, we observe second order h -convergence of the coupled response \mathbf{z} in the $W(0, T)$ space-time norm. Surprisingly, this is not hampered by the convergence of the fluid load (see eq. 2.22)

$$\mathbf{w} \mapsto \int_0^T \int_0^L \mathbf{w}(t, s) \cdot (p \circ \mathbf{z}(t, s) \operatorname{rot} D\mathbf{z}(t, s)) ds dt.$$

which is expected to exhibit $O(h)$ convergence, as p depends on the Γ -gradient of $\phi \in \mathbb{F}^h$, the space of piece-wise linears. We conjecture that the higher-order rate of convergence is caused by the symmetry of the configuration. To verify this conjecture, we consider the following case. A hierarchy of nested meshes and corresponding linear spaces is generated on each level. The pancake geometry of figure 2 and fabricated boundary conditions are projected onto the coarsest mesh. In this case the boundary conditions are $g = \mathbf{z}' \cdot \mathbf{n}$ with

$$\mathbf{z}' = \{0.3(|x_1| - r/2), 0\}, \quad (4.2)$$

thus, g both satisfies the compatibility constraint (2.23) and respects the structural boundary conditions. These projections form the input of the fluid problems that are solved at each mesh level. This ultimately yields the desired family of load functionals that can be tested against the projection of

$$\mathbf{w} = \{0, \sin(k\pi s/L)\},$$

onto a Hermite space on the finest mesh. Note that the test function is thus identical at each resolution of the convergence analysis, eliminating the effect of this projection on observed convergence rates. The cases $k = 1$ and 2 correspond to symmetric and asymmetric test functions \mathbf{w} , respectively.

Employing a hierarchy of equidistant meshes with $16 \cdot \{2, \dots, 15, 60\}$ elements, and comparing the errors with respect to the finest approximation, we obtain the convergence behavior in figure 5. Note that the three curves corroborate the above assertions, namely, that the pressure converges with rate 1 in the $\mathbf{L}^2(0, L)$ norm, but that the rate increases to 2 in the case of a symmetric \mathbf{w} . This enables

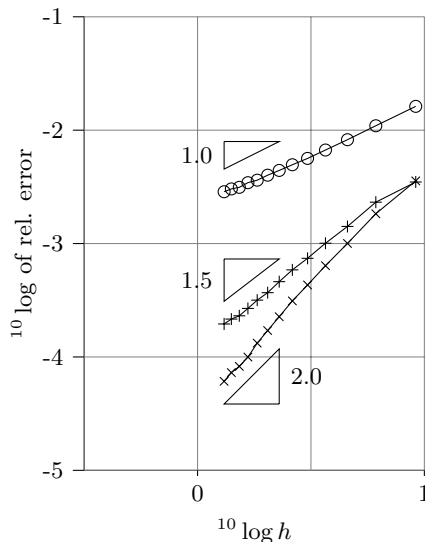


Figure 5: Convergence of the pressure in the $L^2(0, L)$ norm (\circ), and corresponding loads tested against symmetric (\times) and asymmetric ($+$) functions.

the structure solution to converge with rate 2 as observed in the symmetric pancake case of §4.1. In the case of an asymmetric \boldsymbol{w} the convergence rate does not attain the optimal value.

4.2 Folded configuration

We next consider a folded configuration (see fig. 6) including contact forces, with parameters $\zeta = 1.0$, $d = 2.0$. The contact force parameters have been chosen to ensure no self-contact occurs throughout the simulations. Figure 7 illustrates that the membrane exhibits significant wrinkling. These wrinkles are caused by the contact force. The contact force plays a dominant role in the structural response, on account of the so-called *Venturi effect*. This Venturi effect pertains to the phenomenon that the pressure decreases in narrow sections of the fluid domain with nonzero flow. This effect is to be compared to the pressure drop in a converging-diverging channel. The pressure drop causes the membrane on the two opposite sides of the converging section to approach, which in turn causes a local narrowing of the fluid domain, and a corresponding strengthening of the pressure drop. In the absence of contact forces, this process would ultimately lead to a local collapse of the membrane. The aforementioned Venturi effect in fact results in a singular attractive force between sections of the membrane. This singular attractive force must be counteracted by a sufficiently strong singular contact force to avoid collapse of the structure. It is to be noted that the Venturi effect is particular for the considered potential-flow model and that, in contrast, Stokes flow displays a repulsive lubrication effect [28].

Figure 8 displays the error in the displacement for time step $6.621 \cdot 10^{-2}$ and mesh widths h in $L/\{160, 280, 320, 400, 480, 640\}$ with the last of these the resolution for the reference solution. A fine h is observed to be necessary to be in the asymptotic convergence regime. We consider the error convergence as $h \rightarrow 0$ in figure 8. We see that we also recover optimal convergence rates in the norm $\|\cdot\|$ in the case of contact forces.

5. Conclusions

A model was presented for the interaction of a membrane with an enclosed fluid described by potential flow. The linearity of the fluid response allows discretization with the BEM. Despite its simplicity,

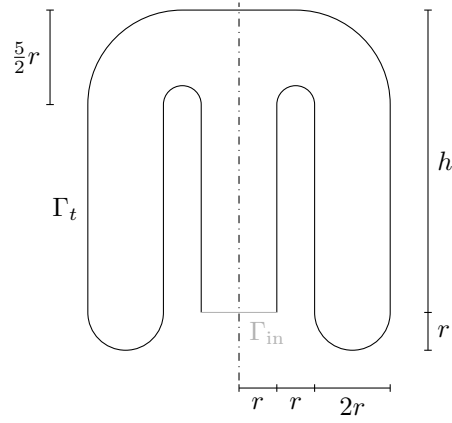


Figure 6: Initial configuration of folded domain test case.

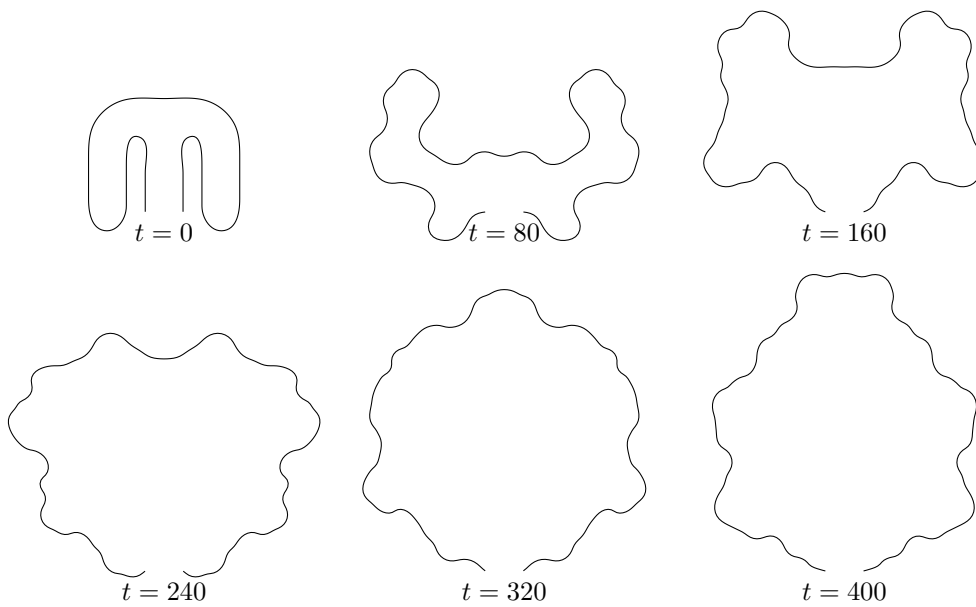


Figure 7: Snapshots of the response for the folded domain.

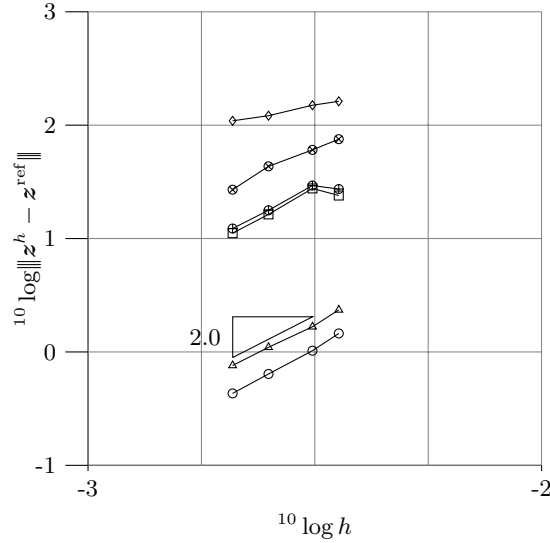


Figure 8: Convergence behavior for the folded configuration in the space-time norm $\|\cdot\|$ with symbols $\{\circ, \triangle, \square, \oplus, \otimes, \diamond\}$ representing time levels $t \in \{0.26, 1.06, 4.24, 16.95, 67.80, 135.59\}$, respectively.

the model poses some theoretical and numerical challenges. Uniqueness results are not available and are not easily acquired. A regularization of the membrane equation is needed for stability. In this work flexural rigidity is introduced for that purpose. As the fluid is enclosed and incompressible, the volume needs to be constrained explicitly. A physical interpretation was derived for the Lagrange multiplier enforcing this constraint, the total internal excess pressure p_0 .

The numerical tests show the capabilities of the presented FE/BE coupling scheme. The discretization of the fluid with the BEM, allows for very large deformations without evolving or recreating volumetric meshes. In this sense, it extends the type of problems that can be treated using an ALE-approach.

To counteract self-crossing of the membrane, ubiquitous in the simulation folded inflatable structures, an efficient contact force is introduced. The potential contact force is passive and its computation is feasible because of reuse of components generated in the BEM formulation of the fluid. An inherent feature of potential flow is the Venturi effect, where pressure forces cause a narrow section in the flow field to contract further. Contraction would lead to collapse and self crossing, which has to be prevented by the contact force. Numerical experiments for a folded configuration revealed that owing to the Venturi effect, the contact forces play a dominant role in the structural response.

6. Acknowledgements

The authors would like to thank Kris van der Zee for fruitful discussions leading to the interpretation of the Lagrange multiplier as a total pressure. This research is supported by the Dutch Technology Foundation STW, which is part of the Netherlands Organization for Scientific Research (NWO) and partly funded by the Ministry of Economic Affairs, Agriculture and Innovation (project number 10476).

A. Nondimensionalization

The membrane motion is given as $s, t \mapsto \mathbf{z} : [0, L] \times [0, T] \rightarrow \mathbb{R}^2$ and governed by

$$\varrho_0 h \mathbf{z}'' = EhD(D\mathbf{z}(1 - |D\mathbf{z}|^{-1})) + (p_0 - \frac{1}{2}\rho|\nabla\phi|^2) \text{rot}D\mathbf{z}, \quad (\text{A.1})$$

with appropriate initial- and boundary conditions. In this equation ϱ_0 , h and E are the membrane density, thickness and stiffness, resp. Furthermore, ρ and ϕ are the fluid density and potential, resp. For nondimensionalization we choose two characteristic quantities of the problem, namely the wave propagation speed in the membrane $c_0 = (E/\varrho_0)^{1/2}$; and a length ℓ , then

$$\mathbf{z} = \ell\{\mathbf{z}\}, \quad \phi = \ell c_0\{\phi\}, \quad (\cdot)' = c_0\ell^{-1}\{(\cdot)'\}, \quad D = \ell^{-1}\{D\}, \quad \nabla = \ell^{-1}\{\nabla\}.$$

In the following, the nondimensionalization braces $\{\cdot\}$ have immediately been dropped. Substitution yields a one-parameter wave equation

$$\mathbf{z}'' - D(D\mathbf{z}(1 - |D\mathbf{z}|^{-1})) - (p_0 - \frac{1}{2}\vartheta|\nabla\phi|^2) \operatorname{rot}D\mathbf{z} = 0, \quad (\text{A.2})$$

with $\vartheta := \rho\ell/\varrho_0h$ the mass ratio. The dimensionless total pressure $\{p_0\} = p_0\ell/(\varrho_0c_0^2h) = p_0\ell/Eh$. Thus, we see that effectively time derivatives have been scaled by c_0 w.r.t. spatial derivatives, i.e., choosing $\ell = 1$ we have $h/1 = \{h\}$ and $\tau \cdot c_0/1 = \{\tau\}$. Secondly, the influence of stiffness is through (i) this scaling of derivatives; and (ii) the total pressure.

For the fluid, we arrive at our old relation,

$$\begin{aligned} \frac{1}{2}\phi(\mathbf{x}) + \frac{1}{2\pi} \oint_{\partial\Omega} \frac{(\mathbf{x} - \mathbf{y}) \cdot \mathbf{n}(\mathbf{y})}{|\mathbf{x} - \mathbf{y}|^2} \phi(\mathbf{y}) d\sigma(\mathbf{y}) &= -\frac{1}{2\pi} \oint_{\partial\Omega} (\log \ell + \log |\mathbf{x} - \mathbf{y}|) h(\mathbf{y}) d\sigma(\mathbf{y}) \\ &= -\frac{1}{2\pi} \oint_{\partial\Omega} (\log |\mathbf{x} - \mathbf{y}|) h(\mathbf{y}) d\sigma(\mathbf{y}), \end{aligned} \quad (\text{A.3})$$

where the last equality follows from the compatibility condition on h .

B. Increased regularity results for the boundary-integral formulation

The aim of this appendix is to establish that under certain simplifying assumptions on the domain, the map $h \mapsto \phi$ corresponding to the boundary-integral formulation (2.3), defines a bounded linear operator from $H^m(\partial\Omega)$ into $H^{m+1}(\partial\Omega)$ ($m \in \mathbb{Z}_+$) and, accordingly, $h \mapsto \nabla_\Gamma\phi$ is a bounded operator from $H^m(\partial\Omega)$ into itself. In light of the analysis in section 2.3, we shall be mostly interested in the case $m = 0$. Below, we first recollect the necessary theory on Fourier characterization of Sobolev spaces, and then proceed by presenting the analysis for a circular domain and, subsequently, discussing extensions to more general domains.

B.1 Fourier characterization of Sobolev spaces

We first recall some elements of the Fourier characterization of Sobolev spaces; see also, for instance, Ref. [3, Ch. 7]. Consider a bounded interval $(0, \Lambda) \subset \mathbb{R}$. We denote by $L^2((0, \Lambda), \mathbb{C})$ the class of square-integrable complex-valued functions, equipped with the inner product

$$(u, v)_{L^2((0, \Lambda), \mathbb{C})} = \int_0^\Lambda u(s) v^*(s) ds, \quad (\text{B.1})$$

where $(\cdot)^*$ denotes the complex conjugate. The norm induced by (B.1) is denoted by $\|\cdot\|_{L^2((0, \Lambda), \mathbb{C})}$. The space $L^2((0, \Lambda), \mathbb{C})$ is a separable Hilbert space. An orthonormal basis of the space is provided by the *Fourier modes*:

$$\{e_n(s) = \Lambda^{-1/2} e^{i2\pi ns/\Lambda}\}. \quad (\text{B.2})$$

Hence, any element $u \in L^2((0, \Lambda), \mathbb{C})$ can be represented with respect to the Fourier-basis functions as

$$u(s) = \sum_{n=-\infty}^{\infty} \hat{u}_n e_n(s) \quad \text{with} \quad \hat{u}_n = (u, e_n)_{L^2((0, \Lambda), \mathbb{C})}. \quad (\text{B.3})$$

Of course, the representation (B.3) holds a fortiori for real-valued functions in $L^2(0, \Lambda) := L^2((0, \Lambda), \mathbb{R})$.

For $u, v \in L^2((0, \Lambda), \mathbb{C})$ it holds that

$$(u, v)_{L^2((0, \Lambda), \mathbb{C})} = \sum_{n=-\infty}^{\infty} \hat{u}_n \hat{v}_n^*. \quad (\text{B.4})$$

The identity (B.4) implies Parseval's theorem,

$$\|u\|_{L^2((0, \Lambda), \mathbb{C})}^2 = \sum_{n=-\infty}^{\infty} |\hat{u}_n|^2, \quad (\text{B.5})$$

and it follows that the Fourier coefficients of functions in $L^2((0, \Lambda), \mathbb{C})$ reside in the space of square summable sequences, $\ell^2(\mathbb{Z})$.

Set $H_p^0(0, \Lambda) := L^2(0, \Lambda)$ and let $H_p^m(0, \Lambda)$ denote the class of periodic functions in $H^m(0, \Lambda)$ ($m \in \mathbb{N}$). For all $k \leq m$ and $n \in \mathbb{Z}$, we have:

$$(D^k u, e_n)_{L^2((0, \Lambda), \mathbb{C})} = \int_0^\Lambda D^k u(s) e_n^*(s) ds = (-1)^k \int_0^\Lambda u(s) D^k e_n^*(s) ds = (\iota \tilde{n})^k \hat{u}_n,$$

where \tilde{n} is a condensed notation for $2\pi n/\Lambda$. Hence, we obtain

$$(u, v)_{H_p^m(0, \Lambda)} = \sum_{k=0}^m \sum_{n=-\infty}^{\infty} (\iota \tilde{n})^k \hat{u}_n ((\iota \tilde{n})^k)^* \hat{v}_n^* = \sum_{n=-\infty}^{\infty} (1 + |\tilde{n}|^2 + \dots + |\tilde{n}|^{2m}) \hat{u}_n \hat{v}_n^* \quad (\text{B.6})$$

and, accordingly,

$$\|u\|_{H_p^m(0, \Lambda)}^2 = \sum_{n=-\infty}^{\infty} (1 + |\tilde{n}|^2 + \dots + |\tilde{n}|^{2m}) |\hat{u}_n|^2. \quad (\text{B.7})$$

B.2 Results for circular domains

We next consider the single- and double-layer potentials conforming to (2.4) for a circular domain of radius r . We consider an arc-length parameterization $(0, \Lambda) \ni s \mapsto \mathbf{x}(s) = r(\cos(s/r), \sin(s/r))$ of the boundary, with $\Lambda = 2\pi r$. Taking the Fourier transform of the right member of the boundary integral formulation (2.3), leads to the following sequence of identities:

$$\begin{aligned} (Vh, e_n)_{L^2((0, \Lambda), \mathbb{C})} &= \int_0^\Lambda e_n^*(s) \int_0^\Lambda G(\mathbf{x}(s), \mathbf{x}(t)) h(t) dt ds \\ &= -\frac{r}{2\pi} \int_0^{2\pi} \int_0^{2\pi} \log r |(\cos \alpha - \cos \theta)^2 + (\sin \alpha - \sin \theta)^2|^{1/2} \frac{e^{-\iota n \alpha}}{\sqrt{\Lambda}} d\alpha h(r\theta) r d\theta \\ &= -\frac{r \log r}{2\pi} \int_0^{2\pi} \frac{e^{-\iota n \alpha}}{\sqrt{\Lambda}} d\alpha \int_0^{2\pi} h(r\theta) r d\theta \\ &\quad - \frac{r}{4\pi} \int_0^{2\pi} \int_0^{2\pi} \log(2 - 2\cos(\alpha - \theta)) \frac{e^{-\iota n \alpha}}{\sqrt{\Lambda}} d\alpha h(r\theta) r d\theta \\ &= -\frac{r \log r}{2\pi} \int_0^{2\pi} e^{-\iota n \alpha} d\alpha \int_0^\Lambda e_0^*(t) h(t) dt \\ &\quad - \frac{r}{4\pi} \int_0^{2\pi} \log(2 - 2\cos \theta) e^{-\iota n \theta} d\theta \int_0^\Lambda e_n^*(t) h(t) dt \\ &= \hat{V}_n \hat{h}_n, \end{aligned}$$

where

$$\hat{V}_n = \begin{cases} -r \log r & \text{if } n = 0, \\ r/(2n) & \text{if } n \in \mathbb{Z} \setminus \{0\}. \end{cases}$$

The collection of eigenvalues $\{\hat{V}_n\}$ is also referred to as the *Fourier symbol* of the single-layer potential. Similarly, we obtain for the Fourier transform of the double-layer potential according to (2.4b):

$$\begin{aligned} (K\phi, e_n)_{L^2((0,\Lambda),\mathbb{C})} &= -\frac{r}{2\pi} \int_0^{2\pi} \frac{e^{-i n \alpha}}{\sqrt{\Lambda}} \int_0^{2\pi} \frac{(\cos \alpha - \cos \theta) \cos \theta + (\sin \alpha - \sin \theta) \sin \theta}{(\cos \alpha - \cos \theta)^2 + (\sin \alpha - \sin \theta)^2} \phi(r\theta) d\theta d\alpha \\ &= \hat{K}_n \hat{\phi}_n, \end{aligned}$$

where the Fourier symbol of the double-layer potential is given by:

$$\hat{K}_n = \begin{cases} -1/2 & \text{if } n = 0, \\ 0 & \text{if } n \in \mathbb{Z} \setminus \{0\}. \end{cases}$$

For given Neumann data $h \in H_{\mathbb{P}}^m(0, \Lambda)$ ($m \in \mathbb{Z}_+$) such that $\oint h = 0$, let ϕ denote the solution to (2.3), subject to the auxiliary condition $\oint \phi = 0$. Taking the Fourier transform of (2.3) and of the auxiliary condition, we obtain that $\hat{\phi}_n = 2\hat{V}_n \hat{h}_n$ for all $n \in \mathbb{Z} \setminus \{0\}$ and $\hat{\phi}_0 = 0$. Hence, the following sequence of inequalities holds:

$$\begin{aligned} \|\phi\|_{H_{\mathbb{P}}^{m+1}(0,\Lambda)}^2 &= \sum_{n \in \mathbb{Z} \setminus \{0\}} (1 + \tilde{n}^2 + \dots + \tilde{n}^{2(m+1)}) |\hat{\phi}_n|^2 \leq 2 \sum_{n \in \mathbb{Z} \setminus \{0\}} (1 + \tilde{n}^2 + \dots + \tilde{n}^{2(m+1)}) |\hat{V}_n|^2 |\hat{h}_n|^2 \\ &\leq r \sum_{n \in \mathbb{Z} \setminus \{0\}} (1 + \tilde{n}^2 + \dots + \tilde{n}^{2m}) |\hat{h}_n|^2 \leq r \|h\|_{H_{\mathbb{P}}^m(0,\Lambda)}^2 \quad (\text{B.8}) \end{aligned}$$

Therefore, it indeed holds that if the Neumann data h in the right member of the boundary integral formulation (2.3) resides in $H_{\mathbb{P}}^m(0, \Lambda)$ ($m \in \mathbb{Z}_+$), then the solution (trace) ϕ lies in $H_{\mathbb{P}}^{m+1}(0, \Lambda)$.

B.3 Extension to non-circular domains

The above results can be extended to non-circular domains which admit an angular parametrization $(0, 2\pi) \ni \theta \mapsto \mathbf{x}(\theta) = r(\theta)(\cos \theta, \sin \theta) \in \mathbb{R}^2$ with $r \in C_{\mathbb{P}}^3(0, 2\pi)$. Let $s(\theta) = \int_0^\theta |D\mathbf{x}(\alpha)| d\alpha$ denote the arc-length coordinate corresponding to the angle θ . We assume that the domain boundary and its parametrization are such that $Ds(\cdot)$ is strictly positive and, accordingly, $s(\cdot)$ does not exhibit stationary points. For the Fourier transform of the single-layer potential in the right member of (2.3), we obtain:

$$(Vh, e_n)_{L^2((0,\Lambda),\mathbb{C})} = \int_0^{2\pi} h(s(\theta)) e_n^*(s(\theta)) \hat{V}_n(\theta) Ds(\theta) d\theta,$$

where

$$\hat{V}_n(\theta) = \int_0^{2\pi} G(\mathbf{x}(\alpha), \mathbf{x}(\theta)) e^{-i\tilde{n}(s(\alpha)-s(\theta))} Ds(\alpha) d\alpha. \quad (\text{B.9})$$

The range of the single-layer potential is determined by the behavior of $\hat{V}_n(\theta)$ in the limit $n \rightarrow \infty$. In the absence of stationary points, Kelvin's stationary-phase argument [37] asserts that as $n \rightarrow \infty$, the only significant contribution to the integral in (B.9) arises from a small neighborhood of the singularity at $\alpha = \theta$. Away from the singularity, the rapid oscillation of $\exp(i\tilde{n}s(\alpha))$ yields an effective destructive interference and, consequently, the overall contribution is $o(n^{-1})$ as $n \rightarrow \infty$. Hence, ignoring terms $o(n^{-1})$, it holds that

$$|\hat{V}_n(\theta)| = \left| \int_{\theta-\varepsilon}^{\theta+\varepsilon} G(\mathbf{x}(\alpha), \mathbf{x}(\theta)) e^{-i\tilde{n}(s(\alpha)-s(\theta))} Ds(\alpha) d\alpha \right| \quad (\text{B.10})$$

as $n \rightarrow \infty$, for any sufficiently small $\varepsilon > 0$. Inserting G in (2.4a) into the above asymptotic approximation, we obtain, successively:

$$\begin{aligned}
|\hat{V}_n(\theta)| &= \left| \frac{1}{4\pi} \int_{\theta-\varepsilon}^{\theta+\varepsilon} \log |r^2(\alpha) + r^2(\theta) - 2r(\alpha)r(\theta) \cos(\alpha - \theta)| e^{-i\tilde{n}(s(\alpha)-s(\theta))} Ds(\alpha) d\alpha \right| \\
&\leq \|Ds\|_{L^\infty(0,2\pi)} \left| \frac{1}{4\pi} \int_{-\varepsilon}^{+\varepsilon} \log |(r^2(\theta) + Dr^2(\theta))\alpha^2 + \rho_0(\alpha)| e^{-i\tilde{n}(Ds(\theta)\alpha + \rho_1(\alpha))} d\alpha \right| \\
&\leq \|Ds\|_{L^\infty(0,2\pi)} \left(\left| \int_{-\varepsilon}^{+\varepsilon} 2 \log |\alpha| e^{-i\tilde{n}Ds(\theta)\alpha} d\alpha \right| \right. \\
&\quad \left. + \left| \int_{-\varepsilon}^{+\varepsilon} \log |(r^2(\theta) + Dr^2(\theta)) + \alpha^{-2}\rho_0(\alpha)| e^{-i\tilde{n}Ds(\theta)\alpha} d\alpha \right| \right)
\end{aligned} \tag{B.11}$$

with ρ_0 the remainder of the Taylor-series expansion of $r^2(\alpha) + r^2(\theta) - 2r(\alpha)r(\theta) \cos(\alpha - \theta) =: \Phi_\theta(\alpha)$ around $\alpha = \theta$ up to second order and ρ_1 the remainder of the Taylor-series expansion of $s(\alpha)$ around $\alpha = \theta$ up to first order:

$$\rho_0(\alpha) = \int_\theta^\alpha \frac{D^3\Phi_\theta(\zeta)}{2} (\alpha - \zeta)^2 d\zeta, \quad \rho_1(\alpha) = \int_\theta^\alpha D^2s(\zeta) (\alpha - \zeta) d\zeta.$$

Note that the remainder ρ_0 contains derivatives of $r(\cdot)$ up to third order. Hence, the remainder is well defined for $r \in C_p^3(0, 2\pi)$. By the stationary-phase argument, the second term in parenthesis in the ultimate expression in (B.11) is $o(n^{-1})$ as $n \rightarrow \infty$. Again ignoring terms $o(n^{-1})$, the first term can be evaluated explicitly:

$$|\hat{V}_n(\theta)| \leq 4 \|Ds\|_{L^\infty(0,2\pi)} \left| \frac{\log \varepsilon \sin(Ds(\theta) \varepsilon \tilde{n}) - \text{Si}(Ds(\theta) \varepsilon \tilde{n})}{Ds(\theta) \tilde{n}} \right|, \tag{B.12}$$

where $\text{Si}(\theta) = \int_0^\theta \alpha^{-1} \sin \alpha d\alpha$ denotes the sine integral. Noting that $\|Ds\|_{L^\infty(0,2\pi)}$ is bounded and that $Ds > 0$ under the standing assumptions, and recalling that $\varepsilon > 0$ is essentially arbitrary, we obtain that $|\hat{V}_n(\theta)| = O(n^{-1})$ as $n \rightarrow \infty$. Hence, in the limit $n \rightarrow \infty$, the single-layer potential behaves essentially the same as in the case of a circular domain.

For the double-layer potential, we have

$$(K\phi, e_n)_{L^2((0,\Lambda),\mathbb{C})} = \int_0^{2\pi} \phi(s(\theta)) e_n^*(s(\theta)) \hat{K}_n(\theta) Ds(\theta) d\theta$$

with

$$\begin{aligned}
\hat{K}_n(\theta) &= -\frac{n_1(\theta)}{2\pi} \int_0^{2\pi} \frac{r(\alpha) \cos \alpha - r(\theta) \cos \theta}{r^2(\alpha) + r^2(\theta) - 2r(\alpha)r(\theta) \cos(\alpha - \theta)} e^{-i\tilde{n}(s(\alpha)-s(\theta))} Ds(\alpha) d\alpha \\
&\quad - \frac{n_2(\theta)}{2\pi} \int_0^{2\pi} \frac{r(\alpha) \sin \alpha - r(\theta) \sin \theta}{r^2(\alpha) + r^2(\theta) - 2r(\alpha)r(\theta) \cos(\alpha - \theta)} e^{-i\tilde{n}(s(\alpha)-s(\theta))} Ds(\alpha) d\alpha.
\end{aligned}$$

We again construct an asymptotic approximation to the above integrals in the limit $n \rightarrow \infty$ by invoking the stationary-phase argument. Accordingly, we obtain

$$\begin{aligned}
\hat{K}_n(\theta) &= -\frac{1}{2\pi} \left(\frac{Dr(\theta) \cos \theta - r(\theta) \sin \theta}{r^2(\theta) + Dr^2(\theta)} n_1(\theta) + \frac{Dr(\theta) \sin \theta + r(\theta) \cos \theta}{r^2(\theta) + Dr^2(\theta)} n_2(\theta) \right) \\
&\quad \times \int_{-\varepsilon}^{\varepsilon} (1/\alpha) e^{-i\tilde{n}(Ds(\theta)\alpha + \rho_1(\alpha))} (Ds(\theta) + \rho_1(\alpha)) d\alpha + o(n^{-1}). \tag{B.13}
\end{aligned}$$

For the components of the normal vector, it however holds that

$$(n_1(\theta), n_2(\theta)) = \frac{\operatorname{rot} D\mathbf{x}(\theta)}{|D\mathbf{x}(\theta)|} = \frac{(r(\theta) \cos \theta + Dr(\theta) \sin \theta, r(\theta) \sin \theta - Dr(\theta) \cos \theta)}{\sqrt{r^2(\theta) + Dr^2(\theta)}} \quad (\text{B.14})$$

and substitution of (B.14) into (B.13) reveals that the term in parentheses vanishes. Hence, we arrive at the result that $|\hat{K}_n(\theta)| = o(n^{-1})$ as $n \rightarrow \infty$.

From the above results, it follows that there exist positive constants C_V, C_K such that:

$$|(Vh, e_n)_{L^2((0,\Lambda),\mathbb{C})}| \leq C_V n^{-1} |\hat{h}_n| \quad |(K\phi, e_n)_{L^2((0,\Lambda),\mathbb{C})}| \leq C_K n^{-1} |\hat{\phi}_n|$$

as $n \rightarrow \infty$. The above asymptotic bounds lead to the following sequence of inequalities:

$$\begin{aligned} \left(\frac{1}{2} - C_K n^{-1}\right) |\hat{\phi}_n| &\leq \frac{1}{2} |\hat{\phi}_n| - |(K\phi, e_n)_{L^2((0,\Lambda),\mathbb{C})}| \leq \left|\frac{1}{2} \hat{\phi}_n - (K\phi, e_n)_{L^2((0,\Lambda),\mathbb{C})}\right| \\ &= |(Vh, e_n)_{L^2((0,\Lambda),\mathbb{C})}| \leq C_V n^{-1} |\hat{h}_n| \end{aligned} \quad (\text{B.15})$$

which implies that $|\hat{\phi}_n| \leq 2C_V n^{-1} |\hat{h}_n|$ as $n \rightarrow \infty$. It then follows from (B.8) that, for the class of domains under consideration, the boundary-integral formulation indeed maps $h \in H_{\mathbb{P}}^m(0, \Lambda)$ ($m \in \mathbb{Z}_+$) to $\phi \in H_{\mathbb{P}}^{m+1}(0, \Lambda)$.

Bibliography

- [1] S. ANTMAN, *Nonlinear problems of elasticity*, Applied Mathematical Sciences, Springer-Verlag, New York, 1995.
- [2] S. S. ANTMAN, *The equations for large vibrations of strings*, The American Mathematical Monthly, 87 (1980), pp. 359–370.
- [3] K. ATKINSON AND W. HAN, *Theoretical Numerical Analysis*, vol. 39 of Texts in Applied Mathematics, Springer, 2010.
- [4] D. BRUNNER, M. JUNGE, AND L. GAUL, *A comparison of fe-be coupling schemes for large-scale problems with fluid-structure interaction*, International Journal for Numerical Methods in Engineering, 77 (2009), p. 664.
- [5] C. CARSTENSEN AND E. STEPHAN, *Adaptive coupling of boundary elements and finite elements*, Mathematical Modelling and numerical analysis, 29 (1995), pp. 779–817.
- [6] F. CIRAK AND R. RADOVITZKY, *A lagrangian–eulerian shell–fluid coupling algorithm based on level sets*, Computers and Structures, 83 (2005), pp. 491–498.
- [7] M. COSTABEL, *Boundary integral operators on Lipschitz domains: elementary results*, SIAM Journal on Mathematical Analysis, 19 (1988), pp. 613–626.
- [8] M. COSTABEL, *Time-dependent problems with the boundary integral equation method*, in Encyclopedia of Computational Mechanics, E. Stein, R. Borst, and T. Hughes, eds., vol. 2: Fundamentals, John Wiley & Sons, Ltd., 2004, ch. 25, pp. 703–721.
- [9] O. CZYGAN AND O. VON ESTORFF, *Fluid-structure interaction by coupling bem and nonlinear fem*, Engineering Analysis with Boundary Elements, 26 (2002), pp. 773–779.
- [10] R. DAUTRAY AND J.-L. LIONS, *Mathematical Analysis and Numerical Methods for Science and Technology*, vol. 6: Evolution problems II, Springer, New York, 1984.
- [11] C. DOMÍNGUEZ, E. STEPHAN, AND M. MAISCHAK, *A fe-be coupling for a fluid-structure interaction problem: Hierarchical a posteriori error estimates*, Numerical Methods for Partial Differential Equations, (2011).

- [12] W. E, *Principles of Multiscale Modelling*, Cambridge University Press, 2011.
- [13] W. ELLEITHY AND R. GRZHIBOVSKIS, *An adaptive domain decomposition coupled finite element-boundary element method for solving problems in elasto-plasticity*, International Journal for Numerical Methods in Engineering, 79 (2009), pp. 1019–1040.
- [14] A. ERN AND J. L. GUERMOND, *Theory and practice of finite elements*, in Applied Mathematical Sciences, S. Antman, J. Marsden, and L. Sirovich, eds., no. 159 in Applied Mathematical Sciences, Springer, New York, 2004.
- [15] L. EVANS, *Partial Differential Equations*, vol. 19 of Graduate Studies in Mathematics, American Mathematical Society, 2009.
- [16] G. N. GATICA, A. MÁRQUEZ, AND M. A. SÁNCHEZ, *Analysis of a velocity–pressure–pseudostress formulation for the stationary stokes equations**, Computer Methods in Applied Mechanics and Engineering, 199 (2010), p. 1064.
- [17] G. HASHIMOTO AND K. ONO, *A fixed eulerian mesh-based scheme using level set function for airbag deployment simulation including the effect of outside air*, in V European Conference on Computational Fluid Dynamics, J. Pereira and A. Sequeira, eds., 2010.
- [18] A. HIRTH, A. HAUFE, AND L. OLOVSSON, *Airbag simulation with LS-Dyna: Past - present - future*, in 6th European LS-Dyna Users' Conference, 2007.
- [19] G. HSIAO AND W. WENDLAND, *Boundary Element Methods: Foundation and Error Analysis*, vol. 1 Fundamentals of Encyclopedia of Computational Mechanics, John Wiley & Sons, Ltd, Chichester, 2004, ch. 12, pp. 339–373.
- [20] T. HUGHES, W. LIU, AND T. ZIMMERMANN, *Lagrangian-Eulerian finite element formulation for incompressible viscous flows*, Computer Methods in Applied Mechanics and Engineering, 29 (1981), pp. 329–349.
- [21] U. KÜTTLER, C. FÖRSTER, AND W. A. WALL, *A solution for the incompressibility dilemma in partitioned fluid–structure interaction with pure dirichlet fluid domains*, Computational Mechanics, 38 (2006), pp. 417–429.
- [22] S. LIAPIS, *An adaptive boundary element method for the solution of potential flow problems*, Engineering Analysis with Boundary Elements, 18 (1996), pp. 29–37.
- [23] J. LIONS AND E. MAGENES, *Non-Homogeneous Boundary Value Problems and Applications I*, Springer-Verlag, Berlin, 1972.
- [24] P.-O. MARKLUND AND L. NILSSON, *Simulation of airbag inflation processes using a coupled fluid structure approach*, Computational Mechanics, 29 (2002), pp. 289–297.
- [25] U. MAYER, A. POPP, A. GERSTENBERGER, AND W. WALL, *3d fluid–structure-contact interaction based on a combined 3D fluid–structure-contact interaction based on a combined XFEM FSI and dual mortar contact approach*, Computational Mechanics, 46 (2010), pp. 53–67.
- [26] W. MCLEAN, *Strongly elliptic systems and boundary integral equations*, Cambridge University Press, 2000.
- [27] J. MONAGHAN, *Smoothed particle hydrodynamics*, in Annu. Rev. Astron. Astrophys., vol. 30, Annual Reviews Inc., 1992, pp. 543–574.

- [28] T. OPSTAL, VAN, E. BRUMMELEN, VAN, R. BORST, DE, AND M. LEWIS, *A finite-element/boundary-element method for large-displacement fluid-structure interaction*, Computational Mechanics, (2012).
- [29] J. RUNGAMORNROT AND M. MEAR, *SGBEM-FEM coupling for analysis of cracks in 3d anisotropic media*, International Journal for Numerical Methods in Engineering, (2011), pp. 224–248.
- [30] P. SAKSONO, W. DETTMER, AND D. PERIĆ, *An adaptive remeshing strategy for flows with moving boundaries and fluid–structure interaction*, International Journal for Numerical Methods in Engineering, 71 (2007), pp. 1009–1050.
- [31] S. SAUTER AND C. SCHWAB, *Boundary Element Methods*, Springer, 2010.
- [32] F.-J. SAYAS, *Weak normal derivatives, normal and tangential traces and tangential differential operators on lipschitz boundaries*. 2009.
- [33] E. STEPHAN, *Coupling of Boundary Element Methods and Finite Element Methods*, vol. 1 Fundamentals of Encyclopedia of Computational Mechanics, John Wiley & Sons, Ltd, Chichester, 2004, ch. 13, pp. 375–412.
- [34] E. P. STEPHAN AND M. MAISCHAK, *A posteriori error estimates for fem-bem couplings of three-dimensional electromagnetic problems*, Computer Methods in Applied Mechanics and Engineering, 194 (2005), pp. 441–452. Selected papers from the 11th Conference on The Mathematics of Finite Elements and Applications.
- [35] K. TAKIZAWA, T. SPIELMAN, AND T. TEZDUYAR, *Space–time FSI modeling and dynamical analysis of spacecraft parachutes and parachute clusters*, Computational Mechanics, 48 (2011), pp. 345–364.
- [36] S. K. VEERAPANENI, A. RAHIMIANY, G. BIROS, AND D. ZORIN, *A fast algorithm for simulating vesicle flows in three dimensions*, Journal of Computational Physics, 230 (2010), pp. 5610–5634.
- [37] G. WHITHAM, *Linear and Nonlinear Waves*, Pure and Applied Mathematics, Wiley, New York, 1974.
- [38] L. WROBEL, *The Boundary Element Method*, vol. 1. Applications in Thermo-Fluids and Acoustics, John Wiley & Sons, 2002.
- [39] D. YONG, *Strings, chains and ropes*, SIAM, 48 (2006), pp. 771–781.
- [40] A. YORK, D. SULSKY, AND H. SCHREYER, *Fluid-membrane interaction based on the material point method*, Int. J. Numer. Meth. Engrg., 48 (2000), pp. 901–924.
- [41] O. ZIENKIEWICZ, D. KELLY, AND P. BETTESS, *The coupling of the finite element method and boundary solution procedures*, International Journal for Numerical Methods in Engineering, 11 (1977), pp. 355–375.